Multiple Bunch Longitudinal Dynamics Measurements at the Cornell Electron-Positron Storage Ring*

R. Holtzapple, M. Billing, and D. Hartill

Laboratory of Nuclear Studies, Cornell University, Ithaca, NY 14853

Abstract

The Cornell Electron-Positron Storage Ring (CESR) has a longitudinal dipole-coupled-bunch instability that limits the total amount of current that can be stored in the ring without feedback. As a result, it is one of the major limitations for higher stored current and luminosity. This paper reports the measurements of multiple bunch longitudinal dynamics done on CESR with a streak camera. The camera was used to measure the dependence of the bunch distribution on current and accelerating RF voltage, for multiple bunches stored in CESR, as well as the effects of the longitudinal instability on the bunch distribution. Measurements of the beam's longitudinal bunch distribution with multiple bunches present in the ring, help give an understanding of the instability, how it affects the bunch distribution, and possibly give insight into a cure of the instability.

1. Multiple Bunch Operations at CESR

Multiple bunches refers to more than one bunch of electrons or positrons being present in CESR at one time. Multiple bunches in CESR are necessary to achieve high luminosity. Under present high energy physics colliding beam conditions, there are up to nine nearly evenly spaced trains of bunches, with up to five bunches in each train, for a maximum of 45 electron and 45 positron bunches. The bunches are separated at crossing points, other than the interaction point, by vertical and horizontal electrostatic separators. The horizontal separators are used to make a "pretzeled" orbit to insure separation between bunch crossings at locations other than the interaction point. The CESR accelerator complex is depicted in Fig. 1.

In CESR, positrons and electrons typically collide at the center of mass energies between 9.4-11.2 GeV. The energy of each beam can be between the energy of 4.7-5.6 GeV but normally CESR is either at 5.289 GeV or 5.269 GeV. The multiple bunch measurements were performed at both energies; one of the consequences of the energies being close together is that the difference in bunch length for these two different energies is negligible. In CESR there are two wiggler magnets, located near the interaction region, which produce synchrotron radiation for the Cornell High Energy Synchrotron Source (CHESS). Opening and closing the wiggler magnets affect the longitudinal phase space of the beam as will be discussed later. There were four normal conducting RF accelerating sections present in CESR when the measurements were performed. Since the measurements have been performed, they have been replaced with superconducting RF sections.

* Work supported by the National Science Foundation.

The measurements were performed on both the electron and positron bunches when the opportunity for beam time was available. Some of the parameters of CESR are shown in table I.

Energy (on/off resonance)	5.289/5.269 GeV
Circumference	768.428 m
Revolution Period	2.563 μsec
RF Frequency	499.765 MHz
Horizontal Tune Qx	10.53
Vertical Tune Qy	9.61
Longitudinal Tune Qs	0.051
Harmonic number	1281

TABLE I. Parameters of the CESR storage ring.

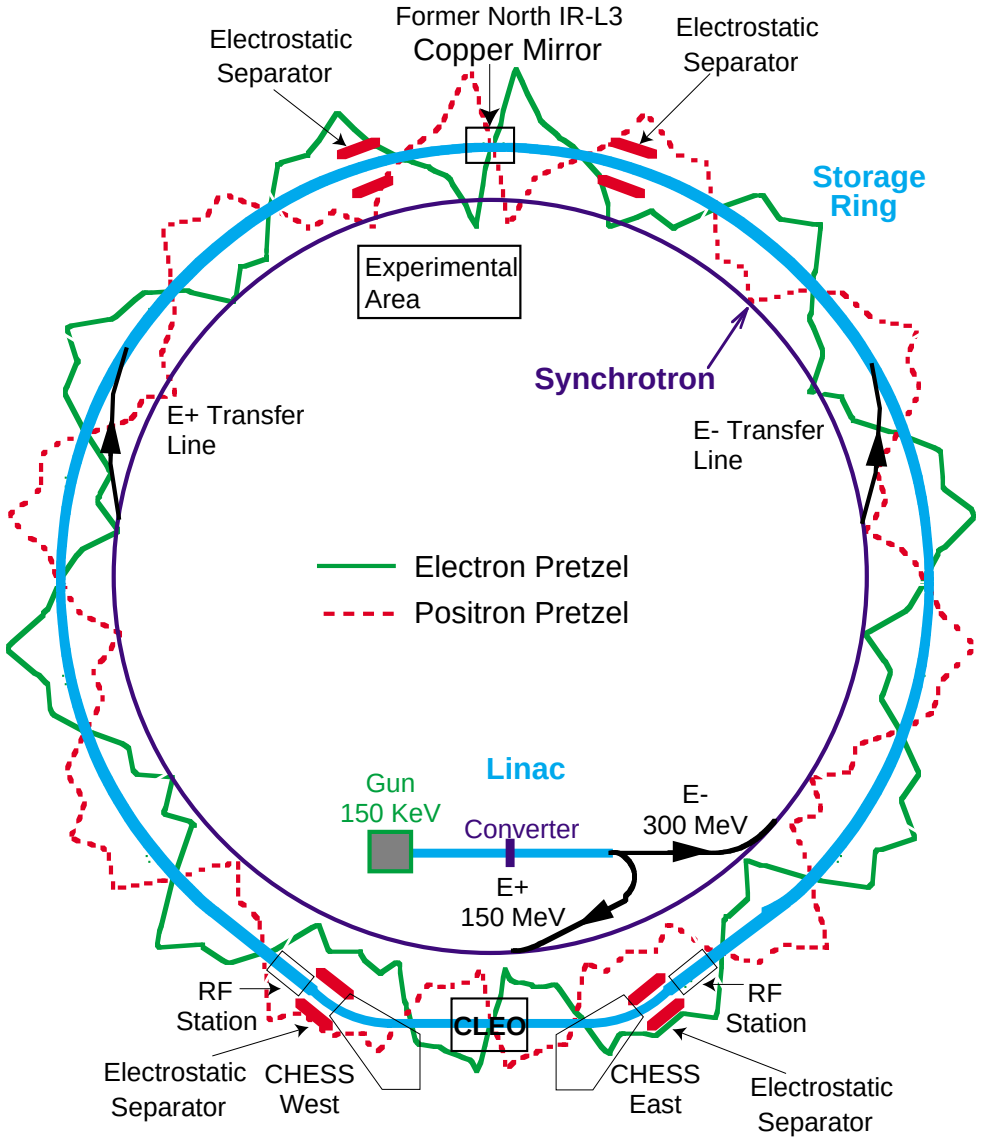

FIG. 1. The layout of the Cornell Accelerator Complex. The streak camera experimental area and the mirror used to reflect the light out of the CESR vacuum chamber is located near the former North interaction region (IR).

During high-energy colliding beam physics at CESR, there are many different possible bunch spacing configurations. The 45 bunches are split into nine trains with each train allowed to have a maximum of five buckets filled. Different spacing of bunches in CESR results in a factor of two variations in the instability threshold (fig. 20 (a)-(c)). At the time of the measurements, the highest total current achieved is with nine trains with two bunches separated by 42 ns (fig. 2).

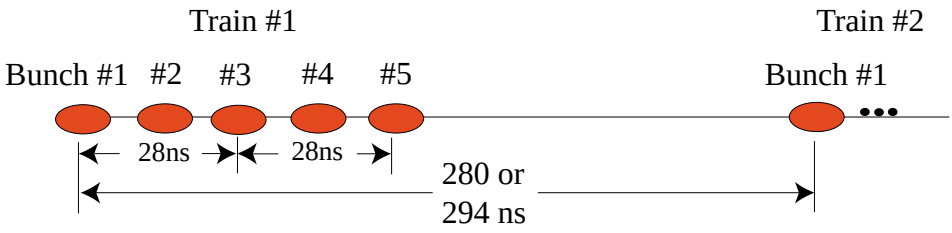

FIG. 2. There are nine trains of bunches in CESR. Each train is separated by 280 or 294 ns and can have up to five bunches per train. The spacing between bunches is 14 ns. The highest luminosity in CESR, at the time of the streak camera measurements, was achieved with bunches #2 and #5 occupied in each train.

For a single bunch in CESR the motion is described by internal electromagnetic fields from the bunch and the external electromagnetic fields from the magnets and the RF system. When the bunch intensity is low, magnets and RF cavity fields determine particle motion. At higher currents beam generated fields do not significantly modify the dynamics so single bunch behavior is stable in CESR [1]. This is not the case for multiple bunches in CESR.

With multiple bunches a dipole-coupled-bunch longitudinal instability is driven by the interaction of the multiple bunches with their vacuum chamber environment. During colliding beams there are many high intensity particle bunches. These high intensity bunches contain a relatively large charge and act as a source of electromagnetic fields, called wakefields, which act back on the beam. As a result the wakefields can cause a change in the synchrotron oscillation frequency, a change in the bunch distribution, or instability. These collective effects can cause collective motion of the many particles in the beam. A detailed description of collective effects is outside of the scope of this paper, a number of papers which cover collective effects are available [2,3].

An alternative description beams' longitudinal phase space can be determined from the beam-generated spectra and compared to the streak camera measurements.

2. Theory

We begin with the longitudinal phase space density, $\rho(\tau,\phi)$, which can be written in action-angle coordinates in terms of the synchrotron oscillation amplitude τ and phase ϕ. The longitudinal phase

space density can depend on τ, but for particles to be independent, it can not depend on ϕ. The longitudinal spectrum of a beam has a beam generated signal given by [4]

$$I(\omega) = \omega_r \sum_{k=-\infty}^{\infty} \sum_{n=-\infty}^{\infty} \delta(\omega - k\omega_s - n\omega_r) \int_0^{\infty} \tau d\tau \int_0^{2\pi} d\phi \rho(\tau, \phi) e^{-ik\phi} J_k(\omega\tau) \quad (1)$$

where ω_r is the revolution frequency, ω_s is the synchrotron frequency, $\rho(\tau, \phi)$ is the phase space density, and J_k is an ordinary Bessel function of order k. In general, the longitudinal bunch density at time t can be written as a Fourier expansion in ϕ

$$\rho(\tau, \phi) = \frac{1}{2\pi} \sum_{m=-\infty}^{\infty} \rho_m(\tau) \mathrm{e}^{im\phi} \quad (2)$$

where τ is the amplitude and ϕ is the phase, and the phase space rotates at frequency ω_s.

At low current, the bunch motion is determined by electromagnetic fields of the accelerator and the beams' generated fields are negligible. As the current increases, the phase space structure is a result of the beams interaction with its own field. The beam-induced field depends on the amount of charge in the bunch and the bunch distribution. It can be concluded from equation 1 that azimuthal structure in longitudinal phase space is present when synchrotron sidebands are observed [4]. These synchrotron sidebands imply azimuthal phase space. Following are examples of beam related signals which relate to the observation of the dipole-coupled-bunch longitudinal instability in CESR.

a) No Perturbation (m=0):

Suppose the beam is not perturbed (m=0) and the phase space density is Gaussian in τ with an rms bunch length σ_τ and uniform in phase ϕ. The phase space is then given

$$\rho(\tau, \phi) = \frac{Q}{2\pi\sigma_\tau^2} \exp\left(-\tau^2 \Big/ 2\sigma_\tau^2\right)$$

which is substituted into equation 1 to give the current spectrum of

$$I(\omega) = Q\omega_r \exp\left(-\omega^2\sigma_\tau^2 \Big/ 2\right) \sum_{n=-\infty}^{\infty} \delta(\omega - n\omega_r).$$

The spectrum observed for the m=0 case is a series of lines located at $\omega = n\omega_r$, with a Gaussian envelope with a rms width of $1/\sigma_\tau$. It should be noted that signals at the synchrotron sideband are not present in this state when the beam has not been excited.

b) Dipole Perturbation (m=$\pm$1):

Now if the beam has a dipole perturbation, the phase space density is given by

$$\rho(\tau, \phi) = \frac{Q}{2\pi\sigma_\tau^2} \exp\left(-\tau^2 \Big/ 2\sigma_\tau^2\right)\left(1 + \mathrm{P}_1 \frac{\tau}{\sigma_\tau} \cos\phi\right) \quad (3)$$

and the resulting beam spectrum is

$$I(\omega) = Q\omega_r \exp\left(-\omega^2\sigma_\tau^2/2\right)\left[\sum_{n=-\infty}^{\infty}\delta(\omega - n\omega_r) + \mathrm{P}_1\frac{\omega\sigma_\tau}{2}\left(\sum_{n=-\infty}^{\infty}\delta(\omega - n\omega_r + \omega_s) + \sum_{n=-\infty}^{\infty}\delta(\omega - n\omega_r - \omega_s)\right)\right]$$

The spectrum consists of two parts. The first part is identical to the unperturbed beam, and the second part is the signal from the dipole perturbation. The dipole signal gives sidebands at $\pm\omega_s$. The phase space of the dipole perturbation is plotted in fig. 3 (a) and (b). Signals at the first synchrotron sideband have been detected at CESR with a spectrum analyzer and the results of the measurement will be presented later in this paper.

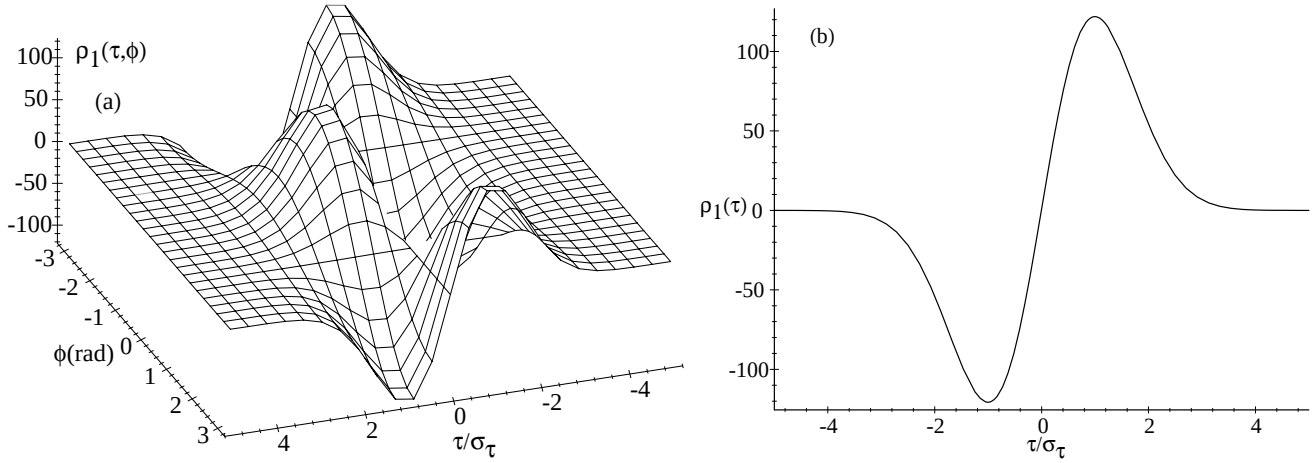

FIG. 3. (a) A phase space plot of the dipole perturbation (equation 3) where $\rho_1(\tau,\phi) = 2\rho(\tau,\phi)\pi\sigma_\tau^2/Q$ and the factor $\mathrm{P}_1 = 200$ for plotting purposes. (b) A two dimensional picture of the bunch distribution in fig. (a) where $\rho_1(\tau) = \rho_1(\tau, \phi = 0)$.

c) Dipole and Quadrupole perturbation (m=±1, ±2):

Suppose the beam has a dipole and quadrupole perturbation, the phase space density is given by

$$\rho(\tau,\phi) = \frac{Q}{2\pi\sigma_\tau^2}\exp\left(-\tau^2/2\sigma_\tau^2\right)\left(1 + \mathrm{P}_1\frac{\tau}{\sigma_\tau}\cos\phi + \mathrm{P}_2\frac{\tau^2}{\sigma_\tau^2}\cos(2\phi)\right) \qquad (4)$$

and the resulting beam spectrum is

$$I(\omega) = Q\omega_r \exp\left(-\omega^2\sigma_\tau^2/2\right)\left[\sum_{n=-\infty}^{\infty}\delta(\omega - n\omega_r) + \mathrm{P}_1\frac{\omega\sigma_\tau}{2}\left(\sum_{n=-\infty}^{\infty}\delta(\omega - n\omega_r + \omega_s) + \sum_{n=-\infty}^{\infty}\delta(\omega - n\omega_r - \omega_s)\right)\right.$$
$$\left. + \mathrm{P}_2\frac{\omega^2\sigma_\tau^2}{2}\left(\sum_{n=-\infty}^{\infty}\delta(\omega - n\omega_r + 2\omega_s) + \sum_{n=-\infty}^{\infty}\delta(\omega - n\omega_r - 2\omega_s)\right)\right]$$

The spectrum consists of the unperturbed part, the dipole perturbation at sidebands at $\pm\omega_s$, and the quadrupole perturbations at sidebands of $\pm 2\omega_s$. The phase space, envelope of the dipole, and quadrupole perturbation, is plotted in fig. 4 (a) and (b). The second synchrotron sideband has been detected also with a spectrum analyzer at CESR, but it is only present when the first synchrotron

sideband is present, so it is not a pure quadrupole mode but a quadrupole mode that has been induced by a dipole mode.

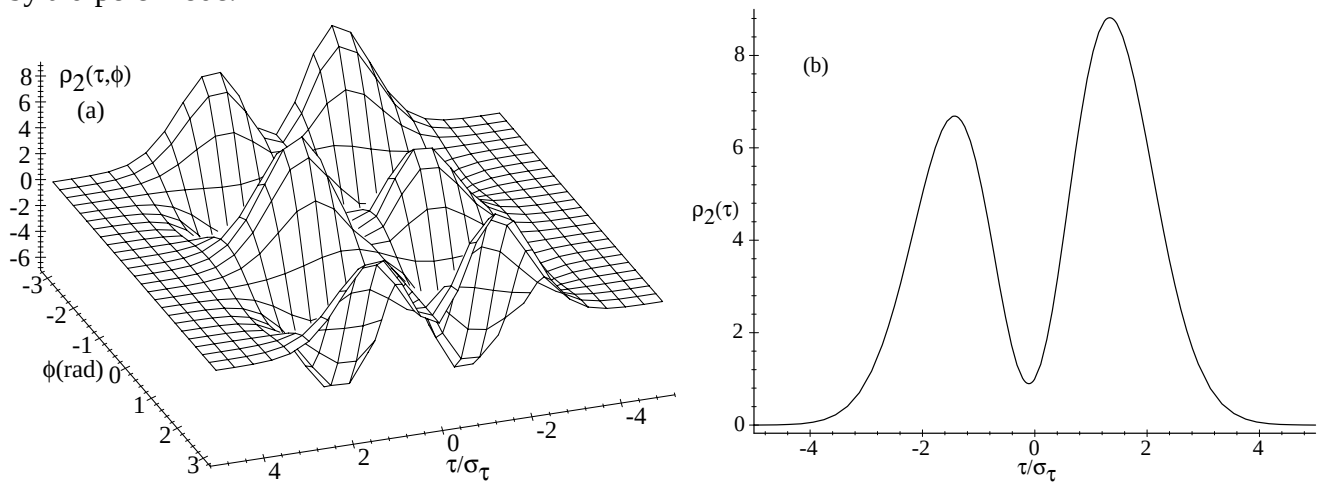

FIG. 4. (a) A phase space plot of the dipole and quadrupole perturbation (equation 4) where $\rho_2(\tau,\phi) = {2\rho(\tau,\phi)\pi\sigma_\tau^2}/{Q}$ and the factors $P_1 = 2$ and $P_2 = 10$. (b) A two-dimensional picture for the bunch distribution in fig. (a) when $\rho_2(\tau) = \rho_2(\tau, \phi = 0)$.

Higher order terms (above the quadrupole mode) have been observed at CESR but they have been either induced or driven from the dipole mode so they are not the primary mode of interest.

3. Streak Camera Data Analysis

Measurements of the CESR longitudinal bunch distribution were made with a 500-femtosecond resolution Hamamatsu streak camera. A detailed description of the camera, experimental set-up, and data analysis techniques are described in detail elsewhere [1]. A brief discussion will be provided here.

To determine the bunch length, the longitudinal profiles of the beam distribution are fit to an asymmetric Gaussian function with a constant background given by

$$I(z) = I_0 + I_1 \exp\left\{-\frac{1}{2}\left(\frac{(z-\bar{z})}{(1+sgn(z-\bar{z})A)\sigma}\right)^2\right\}$$

where I_0 is the background pedestal, and I_1 is the peak of the asymmetric Gaussian. The term $sgn(z-\bar{z})A$ is the asymmetry factor that parameterized the shape of the asymmetric Gaussian. The longitudinal profiles of the beam distribution are χ^2 minimized using the minimization package Minuit [4]. A χ^2 minimization was performed on each streak camera picture

$$\chi^2 = \sum_i^n \frac{\left[I(z_i; A, I_0, I_1, \bar{z}, \sigma) - x_i\right]^2}{x_i}$$

where x_i is the digitized signal from the ith pixel (i=1 to 512) of the streak camera profile and z_i is determined from the fit to the asymmetric Gaussian function. The fit will return the mean $\bar{z}$, asymmetry factor A, background level I_0, peak of the asymmetric Gaussian I_1, and width σ of the distribution. Figure 6 is an example of a streak camera profile fit to the asymmetric Gaussian distribution. The pertinent information retrieved from the asymmetric Gaussian distribution is the rms width

$$\sigma_z = \text{rms width} = \left\langle \left(z - \langle z \rangle\right)^2 \right\rangle^{1/2} = \left[1 + \left(3 - \frac{8}{\pi}\right)A^2\right]^{1/2} \sigma,$$

the mean of the distribution

$$\langle z \rangle = \text{mean} = \bar{z} + 2\sqrt{\frac{2}{\pi}} A\sigma$$

and the asymmetry factor A. These quantities are the quoted results from the measurements.

Many experiments were performed on CESR under different machine parameters. During each experiment, a set of data, which consists of at least ten streak camera pictures, was taken under the same accelerator conditions. The mean rms width, σ_z, and asymmetry factor, A, from each experiment are used to examine the pulse to pulse fluctuations in the beam distribution. Each streak camera distribution is fit to the mean rms width and asymmetry factor where the area and mean position of the asymmetric Gaussian distribution vary. The difference, or residual, between the fit and the data will show variations between an average distribution and individual pictures. The residual, R_{ji} is the ith pixel from the experiment with j streak camera profiles. The residual is determined from the expression

$$R_{ji} = x_i - I\left(z_i; \bar{A}, I_0, I_1, \bar{z}, \bar{\sigma}\right)$$

where $I\left(z_i; \bar{A}, I_0, I_1, \bar{z}, \bar{\sigma}\right)$ is determined by doing a χ^2 fit to the asymmetric Gaussian distribution using the mean sigma ($\bar{\sigma}$) and mean asymmetry factor ($\bar{A}$) from a given experiment, and x_i is the data from the ith pixel. The mean ($\bar{z}$), pedestal I_0, and peak (I_1) of the expression $I\left(z_i; \bar{A}, I_0, I_1, \bar{z}, \bar{\sigma}\right)$ are the fit variables. Figure 7 is an example of a distribution, fit to the mean distribution, and the residual was computed from the fit to the data.

The residuals from each experiment can also be summed to give the mean residual. The mean residual from an experimental data set is determined by summing all the individual residuals in the data set. Because each profile has a different mean position, the residual from each profile is shifted so the mean of the asymmetric Gaussian is at the origin. The residual pixel intensity from each profile is then summed and averaged in two psec bins to remove the granularity of the calibration curve. The mean residual for the jth two ps bin is given by

$$\bar{R}_{ji} = \frac{\sum_{j=1}^{m} \left(x_i - I\left(z_i; \bar{A}, I_0, I_1, \bar{z}, \bar{\sigma}\right)\right)}{m}$$

where $I\left(z_i;\overline{A},I_0,I_1,\bar{z},\overline{\sigma}\right)$ is the asymmetric Gaussian fit to the data when the mean rms width and asymmetry value is held constant. M is the number of pictures taken during the experiment that fit in the two psec bin. Figure 14 is an example of the mean residual from an experiment.

The following sets of multiple bunch measurements were made on CESR with the streak camera: 1) the bunch distribution as a function of current, 2) the bunch length as a function of RF accelerating voltage, 3) the bunch distribution during High Energy Physics collisions, 4) the bunch length with wiggler magnets open and closed, 5) the bunch distribution when modulating the RF voltage, and 6) the bunch distribution with the longitudinal dipole-coupled-bunch instability present under different bunch spacings. These experiments will be presented with comments about the results of the experiment will be discussed in each section.

4. CESR Multiple Bunch Longitudinal Dynamics Measurements

(I) Bunch Distribution as a function of Current

The electron bunch distribution as a function of current was measured with nine trains of two bunches per train present in CESR. For this experiment the bunch length of the first bunch in the train was measured and the separation between the two bunches was 42 ns. During the measurements the wiggler magnets were closed and the bunch had a pretzel orbit. The total beam current was varied from approximately 18 mA to 216 mA and the RF accelerating voltage was set at $6.54 \pm 0.01\text{MV}$. Ten streak camera pictures at each current and fitting the distributions to an asymmetric Gaussian function. Plotted in fig. 5 (a) and (b) is the mean and the root mean error of the bunch width and asymmetry factor at each current setting.

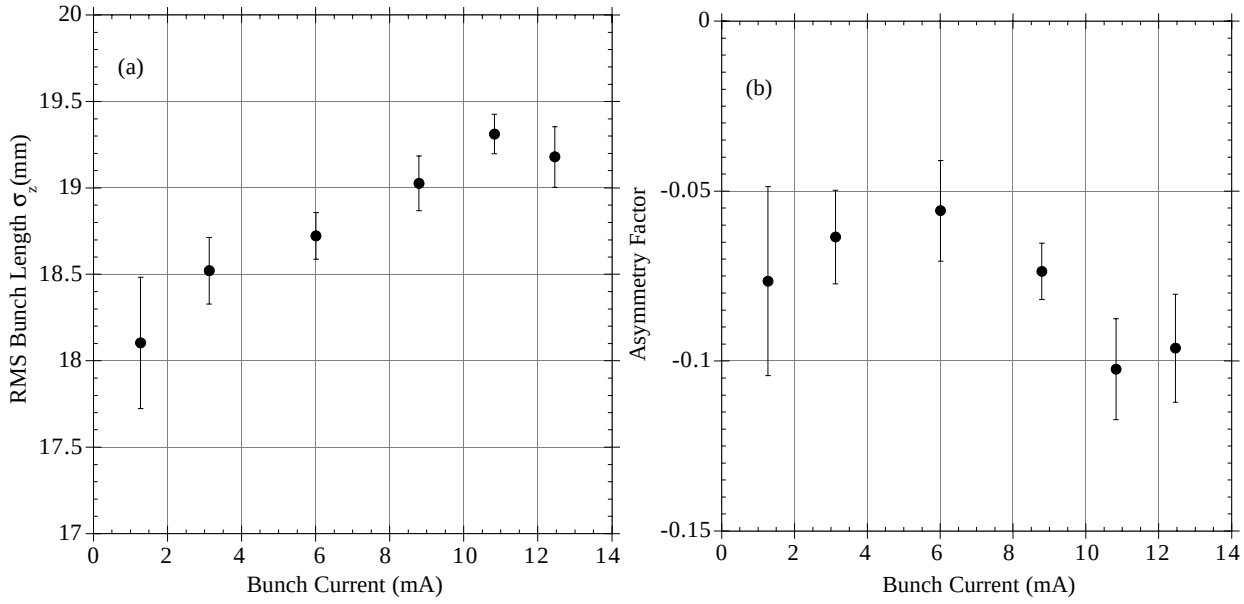

FIG. 5. The electron (a) bunch length as a function of current with 18 bunches in the CESR ring. The (b) asymmetry factor as a function of current.

A single picture of the longitudinal bunch distribution for three different current settings is plotted in fig. 6 (a) through (c).

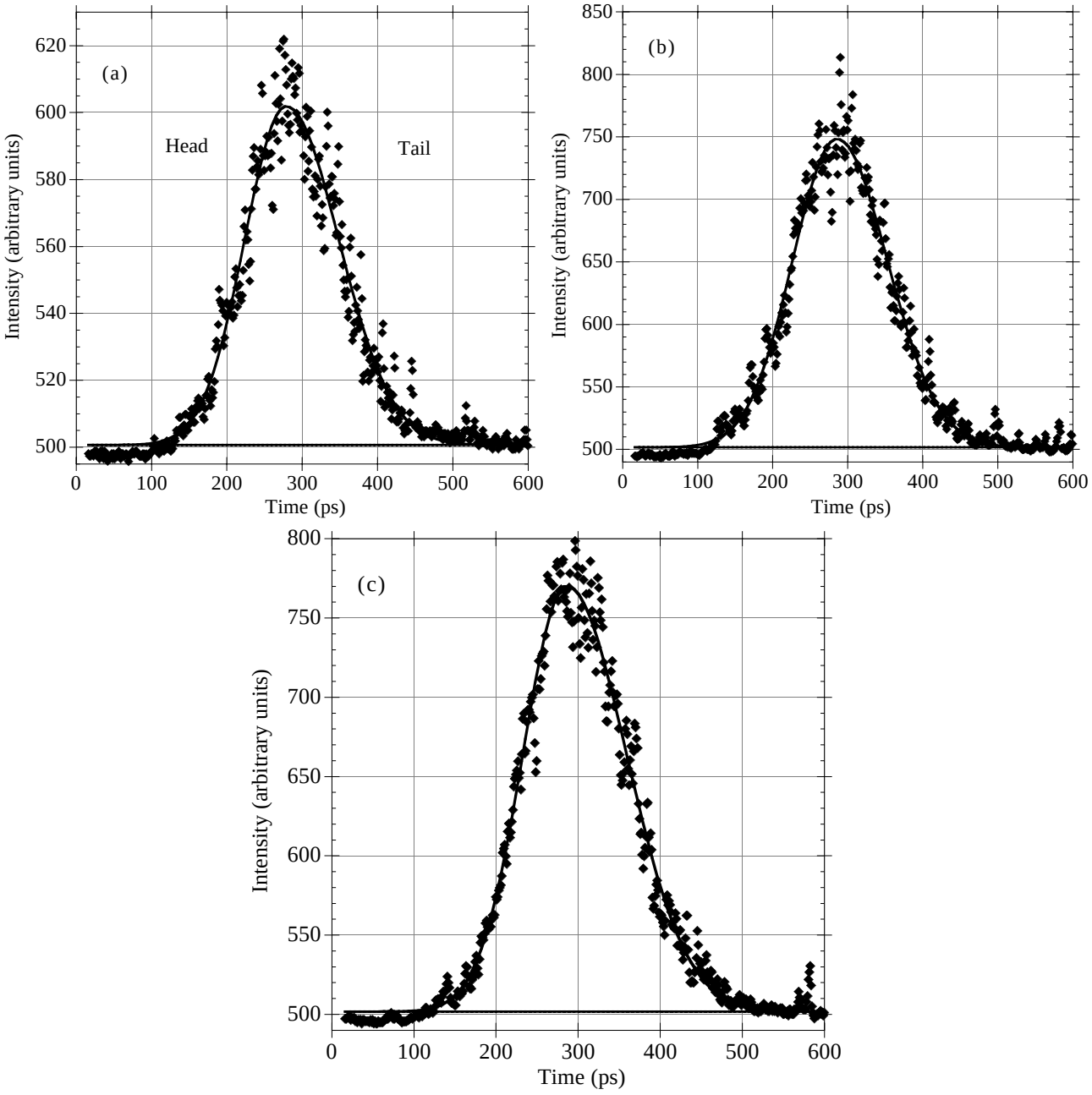

FIG. 6. A single data acquisition of the electron longitudinal bunch distribution at the current settings of: (a) 1.3 mA per bunch, (b) 6.0 mA per bunch, and (c) 12.5 mA per bunch. As denoted in figure (a), the head of the distribution is to the left of the center and the tail of the distribution is to the right of the center of the distribution.

Several observations can be made from the results:

1) Between the current of 1 to 13 mA per bunch, the electron bunch length increases by approximately 6.0%. This steady increase is not accompanied by an increase in the asymmetric Gaussian asymmetry factor. Unlike the single bunch case, the asymmetry factor does not change as a function of current in the multiple bunch case [1].

2) For a single bunch, the bunch length at low current is expected to be $\sigma_z = 17.3\text{mm}$ as calculated for the parameters of CESR. It has been measured at low current to be $\sigma_z = 17.9 \pm 0.35\text{mm}$ which is consistent with the multiple bunch measurement at low current of $\sigma_z = 18.1 \pm 0.38\text{mm}$ [1].

3) The lack of light intensity for the streak camera was a problem at low current. It was necessary to open up the streak camera slit aperture to $300\mu\text{m}$ to allow enough light for the measurement. The $300\mu\text{m}$ aperture resolution correction was made on these measurements.

4) During these measurements the longitudinal instability was not detected by the streak camera or in the beam spectra. At this bunch spacing the threshold current of the dipole-coupled-bunch longitudinal instability is approximately 240 mA for a single beam. Figures 7 (a) through (c) are plots of the distribution fit to the mean distribution with the width and asymmetry factor held constant. Above the distribution, the residual from the fit to the data is plotted. It is evident that there is no greater than a 4% difference between the mean and actual distribution. The longitudinal instability will be discussed later.

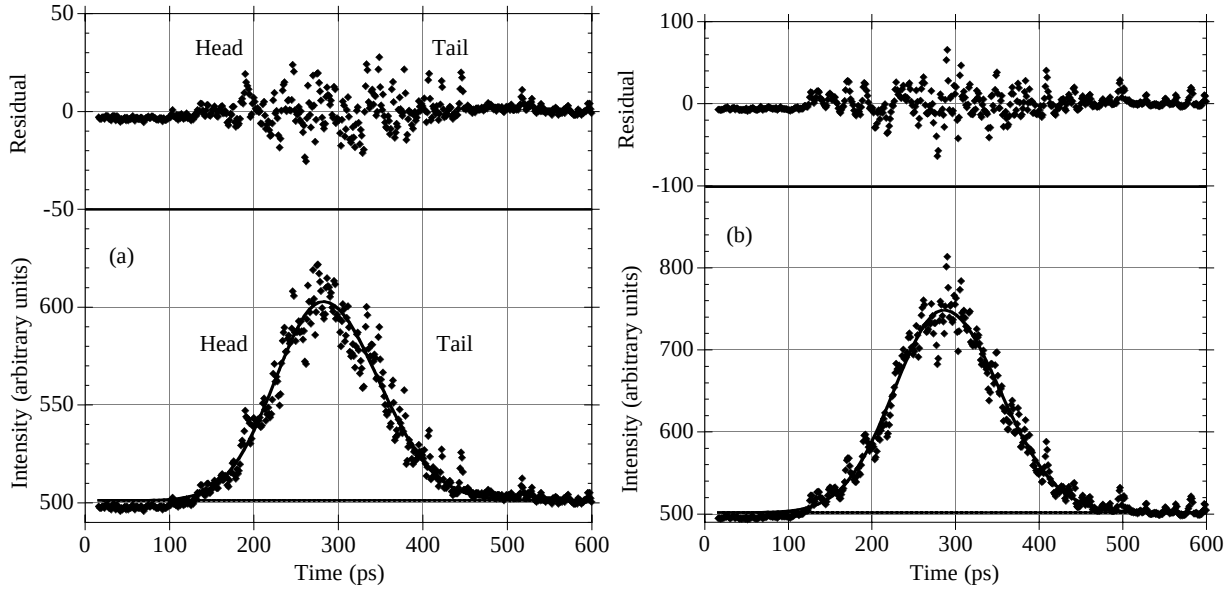

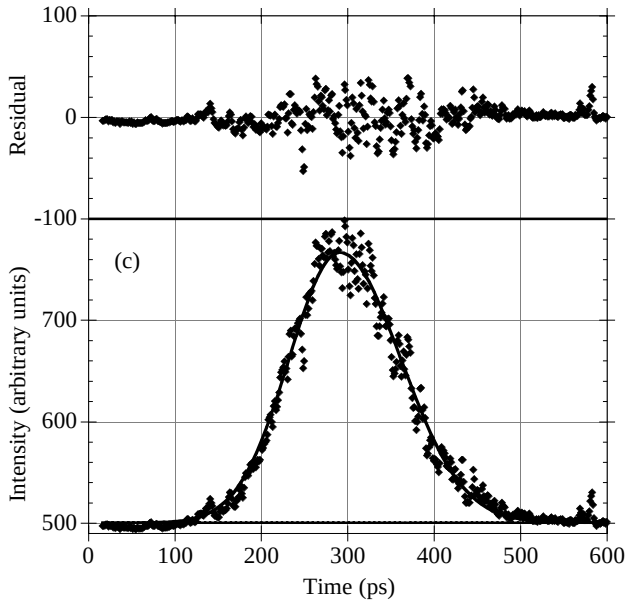

FIG. 7. A single data acquisition of the electron longitudinal bunch distribution fit to the mean distribution with the rms width and asymmetry factor kept constant. The residual from the distribution is plotted above the distribution for the current for the settings of: (a) 1.3 mA per bunch, (b) 6.0 mA per bunch, and (c) 12.5 mA per bunch.

(II) Bunch Length as a function of the RF Accelerating Voltage

The electron bunch length was measured as a function of the RF accelerating voltage. At each RF voltage setting ten streak camera pictures were taken with a constant current in CESR. A measurement was made at high (9mA per bunch), and low (3.2 mA per bunch) current, with nine trains of two bunches separated by 42 ns. Plotted in fig. 8 (a) and (b) is the mean bunch width and root mean error at each RF voltage setting.

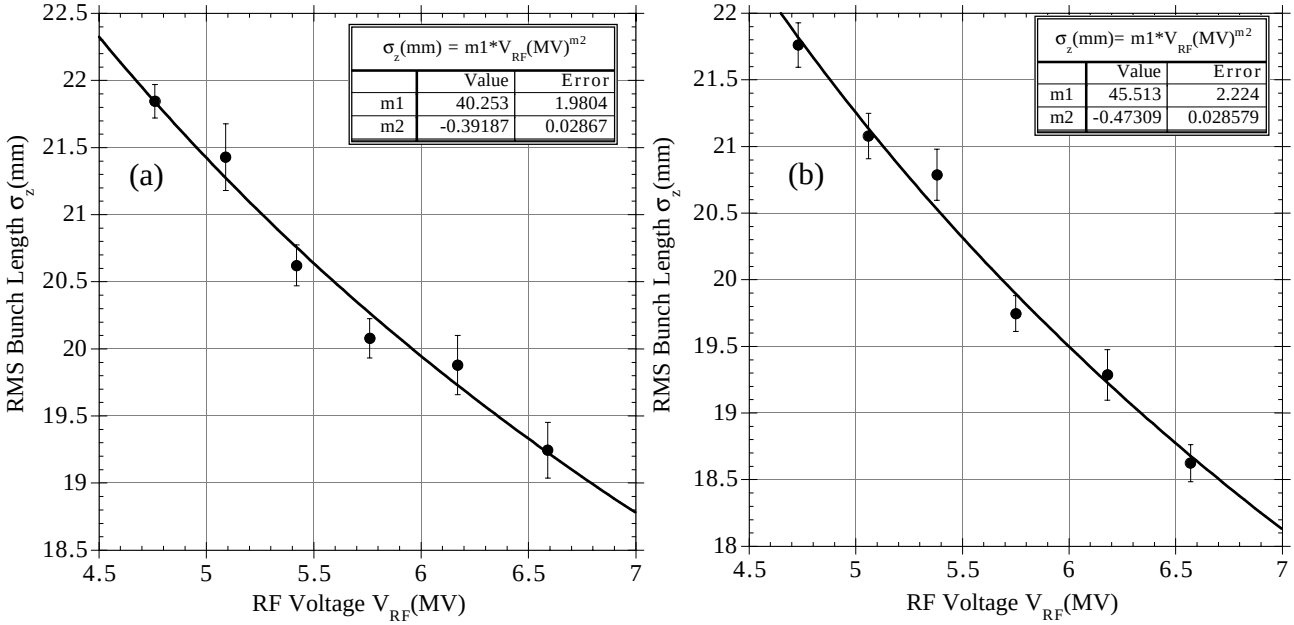

FIG. 8. The electron bunch length as a function of RF accelerating voltage with 18 bunches in the CESR Ring at a current of (a) 9.0 mA per bunch and (b) 3.2 mA per bunch.

Several comments can be made about this experiment:
1) Fitting the data to the equation $\sigma\left(V_{rf}\right) = AV_{rf}^{m}$ the electron bunch lengths' dependence on RF accelerating voltage was determined under the assumption that the voltages for all cavities are in phase. In the low current case, the fit gives $m = -0.47 \pm 0.03$, in the high current case, the fit give $m = -0.39 \pm 0.03$. From single bunch measurements low current behavior of the bunch length is not precisely inversely proportional to the square root of the RF accelerating voltage and at high current, the bunch length dependence on RF voltage deviates from the low current case slightly due to collective effects [1]. Similar behavior is observed in multiple bunch measurements.
2) As expected, the bunch length is shortened as the RF acceleration voltage increases. At the highest RF voltage of 6.6 MV, the difference in bunch length for the low and high current cases is approximately 3%.
3) The dipole-coupled-bunch longitudinal instability was not observed in the bunch distributions or the beam spectra during these measurements.

(III) Bunch Distributions during High Energy Physics Collisions

The bunch distribution was measured for both electrons and positrons as a function of current during high-energy collisions. The measurements were made with nine trains of two bunches with 42 ns spacing. Streak camera pictures were taken of the first bunch in the train when the beams were colliding. Simultaneous detection of the bunch distribution for electrons and positions is not possible, so no correlation between the beams can be inferred. The bunch length and asymmetry factor is plotted as a function of the current in fig. 9 (a) and (b) for electrons and fig. 10 (a) and (b) for positrons.
Several observations can be made from the measurements:
1) The bunch length, for both the electrons and positrons, increases as a function of current. At the time of these measurements, the total peak current collided during high-energy physics was 170 mA per beam. Each fill of CESR would last 70 minutes, or until the single beam current was 120 mA, then CESR was refilled.
2) For both electron and positrons the magnitude of the asymmetry factor increases as a function of current. The asymmetry behavior for a single bunch is also observed with multiple bunches.
3) The measurements of electron and positron bunch lengths' were made on different fills, so it is hard to make any direct comparisons. From the linear fit to the data, it is evident that the bunch length at the beginning, and end of the fill is virtually the same for both beams. Overall, the electrons and positrons exhibit the same behavior in CESR.
4) At a bunch spacing of 42 ns the electron bunch length for the first and second bunch in the train was measured during colliding beams. The results are plotted in fig. 11 (a) and (b). Each data point is the mean and rms error of 20 streak camera pictures. The bunch length for the first bunch in the train is consistently slightly longer as a function of current than the second bunch in the train. The

bunch lengths increase as a function of current. The asymmetry factor of the two bunches closely match each other, and they both increase with current.

5) A dipole-coupled-bunch longitudinal instability was not observed in the bunch distribution or the beam spectra during these measurements.

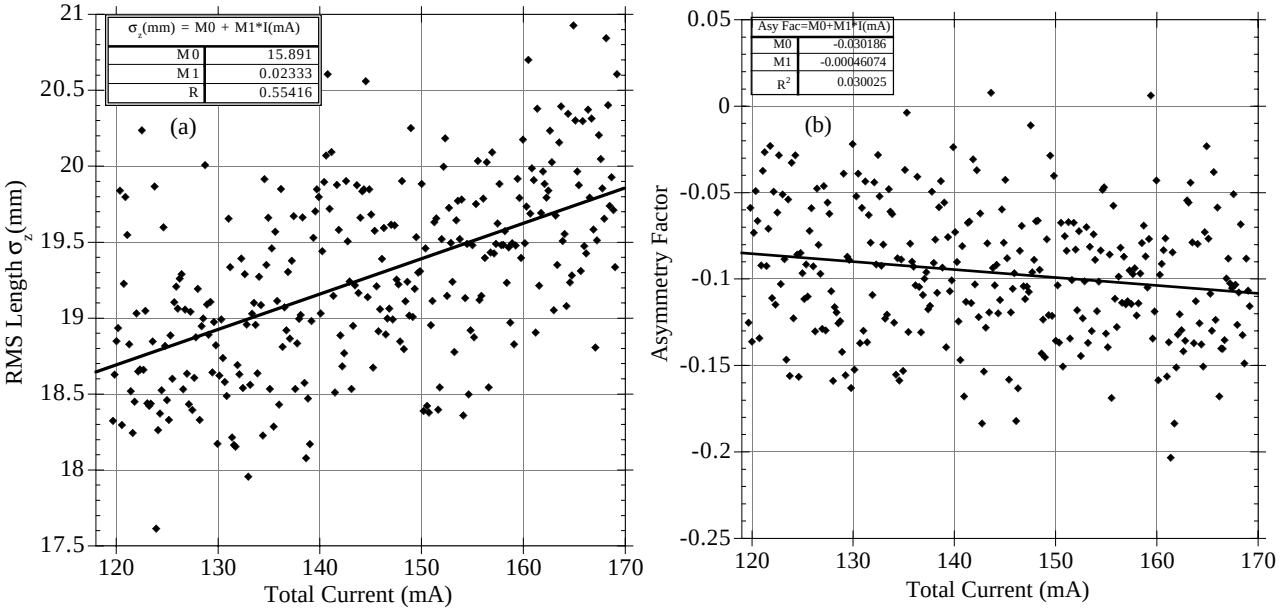

FIG. 9. The electron (a) bunch length and (b) asymmetry factor as a function of current during high-energy collisions in CESR. The fit to the data is linear and points out the slow decrease in the bunch length and asymmetry factor as a function of current. The RF accelerating voltage during the measurement was $6.49 \pm 0.01 \mathrm{MV}$.

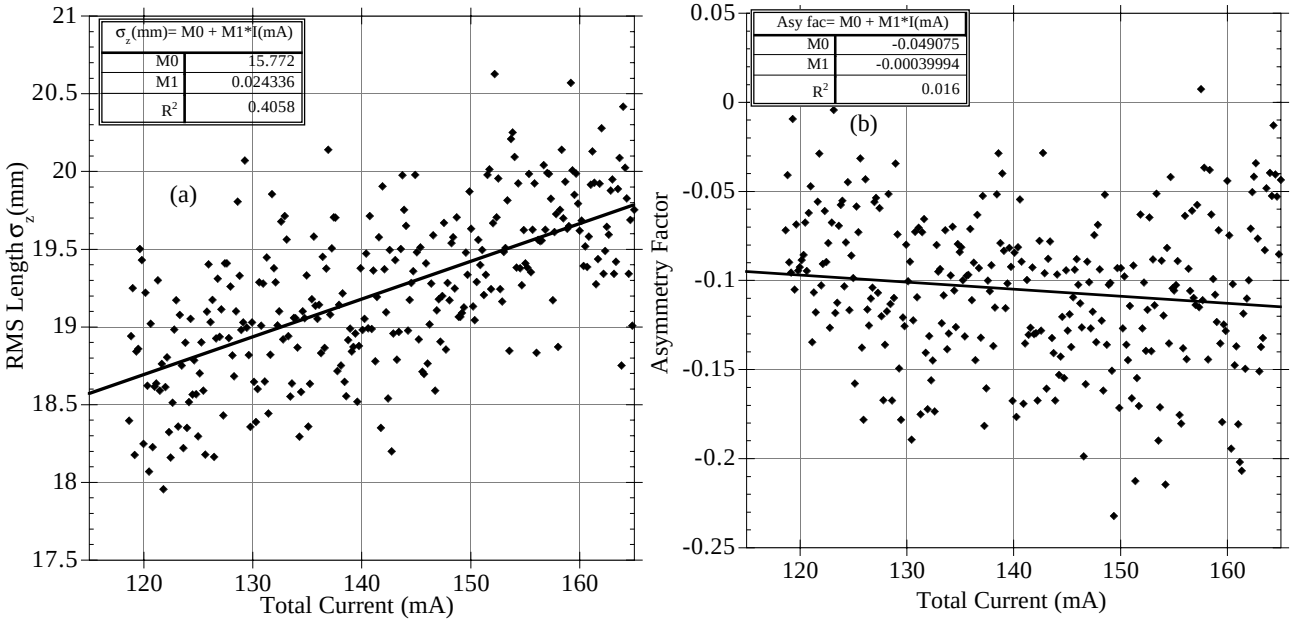

FIG. 10. The positron (a) bunch length and (b) asymmetry factor as a function of current during high-energy collisions in CESR. The bunch length and asymmetry factor is fit to a line. The RF accelerating voltage during the measurement was $6.42 \pm 0.01 \mathrm{MV}$.

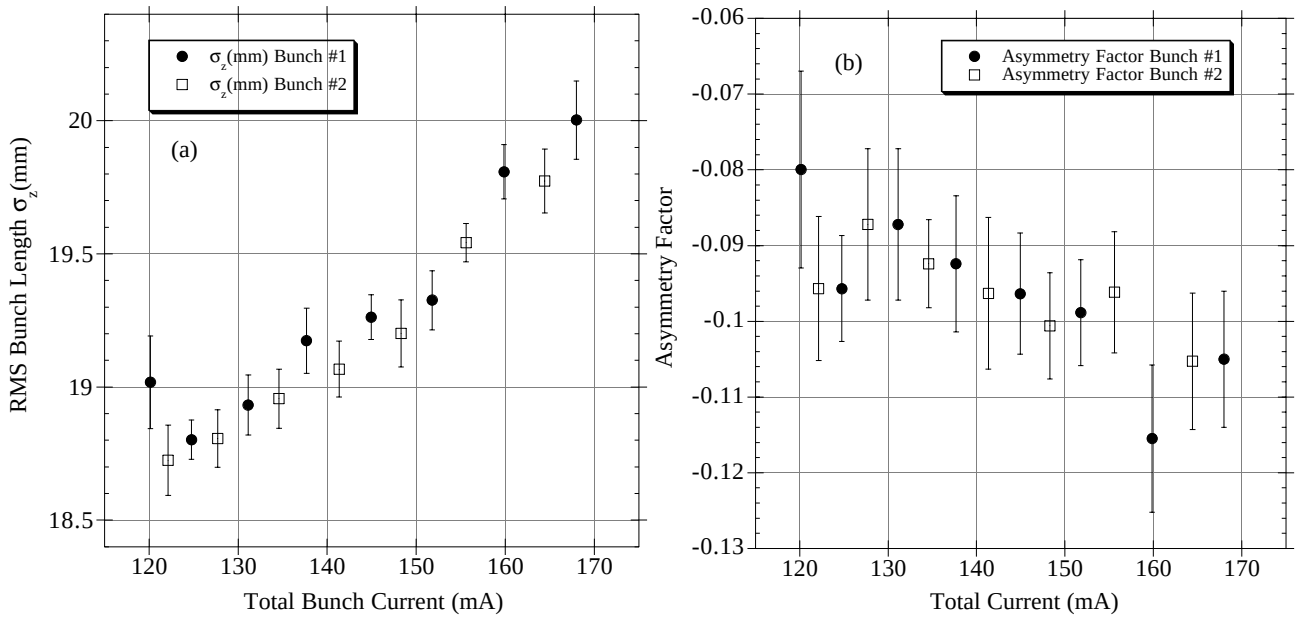

FIG. 11. The electron (a) bunch length and (b) asymmetry factor for bunches one and two as a function of current during high-energy colliding beams. There are 42 ns of spacing between each bunch during the measurement.

(IV) Bunch length measurement with varying pretzel orbit and wiggler magnet

The dependence of the longitudinal bunch distribution on the wiggler magnets and pretzel orbit amplitude was measured with multiple bunches present in CESR. The positron bunch distribution was measured with nine trains with two bunches in each train separated by 42 ns. The RF accelerating voltage was $V_{RF} = 6.89 \pm 0.01\text{MV}$ during the measurements. The measured bunch length and asymmetry factor as a function of pretzel amplitude and wiggler magnets is listed in table II. Figure 12 is a plot of the bunch length as a function of pretzel amplitude.

Horizontal Pretzel Amplitude (CU)	Wigglers Open/Closed	RMS Bunch Length σ_z(mm)	Asymmetry Factor
0	open	17.44 ± 0.09	-0.10 ± 0.01
0	closed	18.53 ± 0.12	-0.13 ± 0.01
1500	open	17.25 ± 0.08	-0.10 ± 0.01
1500	closed	18.17 ± 0.10	-0.10 ± 0.01
2500	open	17.20 ± 0.07	-0.10 ± 0.01
2500	closed	18.27 ± 0.07	-0.09 ± 0.01
2800	open	17.10 ± 0.07	-0.11 ± 0.01

Table II. The positrons bunch length and asymmetry factor of the CESR bunch distribution as a function of pretzel amplitude with wiggler magnets open and closed. The horizontal pretzel amplitude units are computer units and the conversion to separation is approximately 1000 CU=1mr for one half of the horizontal crossing angle at the interaction point.

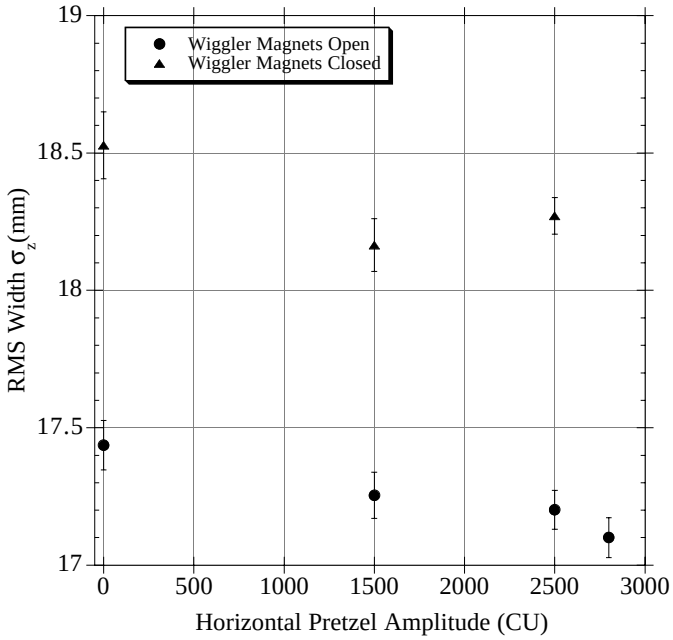

FIG. 12. The positron bunch length with the wiggler magnets open and closed as a function of the horizontal pretzel orbit amplitude.

It can be concluded that the pretzel amplitude does not significantly change the bunch length or asymmetry factor appreciably. The wiggler magnets change the bunch length by approximately 6% with zero horizontal separation and with full pretzel amplitude (2500 CU).

(V) Modulation of the RF Accelerating Voltage

Modulating the phase or amplitude of the RF voltage with a single bunch produces longitudinal collective motion of the bunch in CESR. The RF accelerating voltage was modulated with a signal generator to observe the redistribution of particles in longitudinal phase space.

A tracking signal generator from a spectrum analyzer having variable amplitude and frequency was used to excite the desired mode of oscillation. When the induced mode of longitudinal oscillation was present, streak camera pictures of the longitudinal bunch distribution were taken. In conjunction a spectrum analyzer recorded the amplitude and frequency of the induced oscillation by observing a beam position signal at a location with non-zero dispersion. Initially under stable conditions, twenty streak camera pictures were taken, to compare the change in the longitudinal distribution with the instability present. The presence of a mode of oscillation is observed as a signal at synchrotron frequency (f_s) sidebands of the rotation frequency (f_r) which is $f_r \pm mf_s$ in the beam spectra. The modes of oscillation induced were the dipole (m=1), quadrupole (m=2), sextupole (m=3), and sextupole modes (m=4). During these measurements the RF accelerating voltage was 6.58 ± 0.01 MV.

a) Dipole Mode (m=1)

The dipole mode of oscillation was induced in CESR in a single bunch of electrons by modulating the phase of the RF voltage at 369.9 kHz when the electron bunch current was approximately 7 mA. To induce the dipole mode the bunch distribution was modulated with signal generator voltage amplitudes of –20 dBm and 10 dBm. Figures 13 (a) and (c) are representative single data acquisitions of the longitudinal profiles of the bunch distribution at these two different voltage amplitudes. The distributions were fit to the mean stable distribution and the residual from the fit is plotted in fig. 13 (b) and (d).

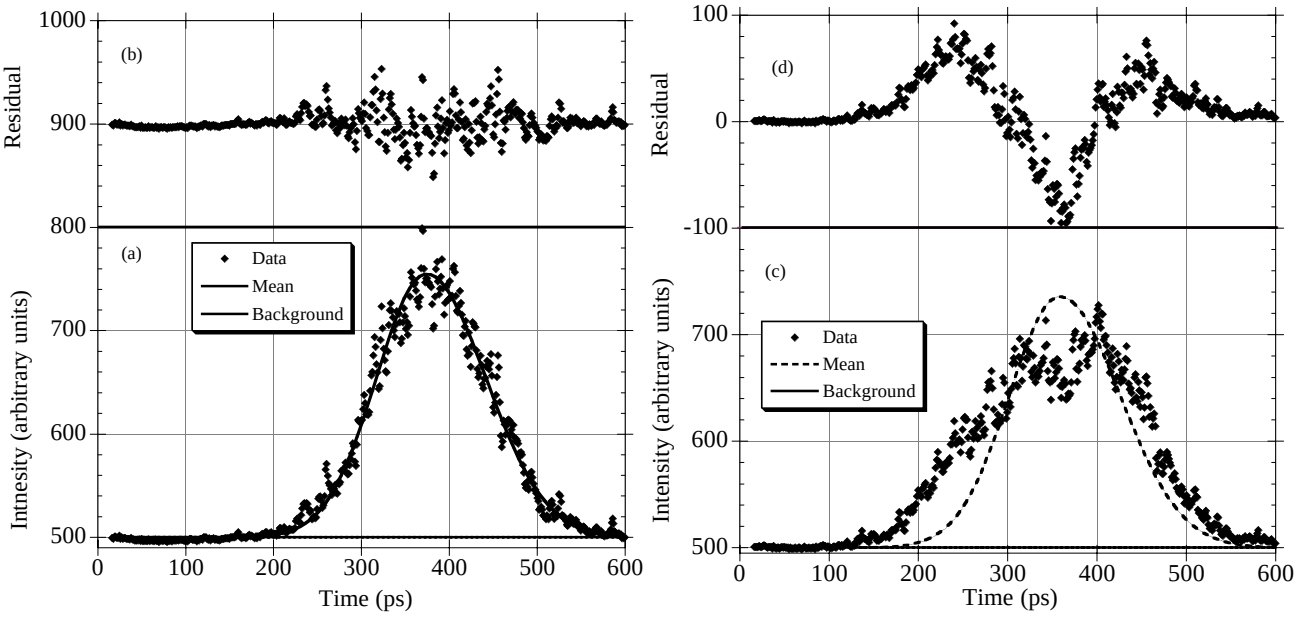

FIG. 13. The CESR electron bunch distributions when the RF phase is modulated at the frequency of 369.9 kHz and signal generator voltage amplitudes of (a) -20 dBm and (b) +10 dBm. The residuals from the mean distribution are plotted above the figure for the signal generator voltages of (c) -20 dBm and (d) +10 dBm.

The frequency and amplitude of the beam spectra measured by the spectrum analyzer while the beam was modulated at 369.9 kHz is listed in table III. The dipole mode signal scaled in direct proportion with the modulation level with a quadrupole mode signal appearing at the higher excitation level.

	-20 dBm Sinewave	+10 dBm Sinewave
f (390 kHz)	-18 dB	-19 dB
$f_r - f_s$ (369.9 kHz, m=1)	-53 dB	-23 dB
$f_r - 2f_s$ (349.9 kHz, m=2)	-	-47 dB

TABLE III. The beam spectra amplitude measured by the spectrum analyzer when modulating the RF voltage at a frequency of 369.9 kHz.

Table IV is the results of the bunch length and asymmetry factor from these measurements. There was no evidence that the longitudinal bunch distribution changed in shape or size when only the $f_r \pm f_s$ signal was present in the beam spectra.

	No Drive	-20 dBm Sinewave	+10 dBm Sinewave
RMS Width σ	18.46 ± 0.11mm	18.34 ± 0.10mm	24.2 ± 0.45mm
Asymmetry Factor	-0.07 ± 0.01	-0.05 ± 0.01	-0.03 ± 0.06

TABLE IV. The electron bunch length and asymmetry factor when RF phase was modulated at a frequency of 369.9 kHz. The error bars for the data is the root mean error of the measurement. The bunch length with no drive and asymmetry value is used in fitting the data to determine the pulse to pulse residual and mean residual from the fit to the data.

Several comments about the induced dipole mode bunch distributions:

1) An oscillation in the arrival time of the bunch distribution is expected with the dipole mode present. The time oscillation has been measured by an oscilloscope to be a few picoseconds in size. A few picosecond time oscillation is in the noise of the streak camera trigger and cannot be measured with the present trigger system.

2) By increasing the modulation voltage amplitude, the signal at $f_r \pm 2f_s$, or the quadrupole mode (m= ± 2) is induced. With the quadrupole mode present the changes in the bunch distribution are large and measurable with the streak camera. The longitudinal shape of the bunch with the quadrupole mode present can be compared to the theoretical phase space density plotted in fig. 4.

3) The mean residual for the two different voltage amplitudes is plotted in fig. 14. There is little evidence of the quadrupole mode structure in the -20 dBm case, and in the +10 dBm case, the quadrupole mode is clearly visible.

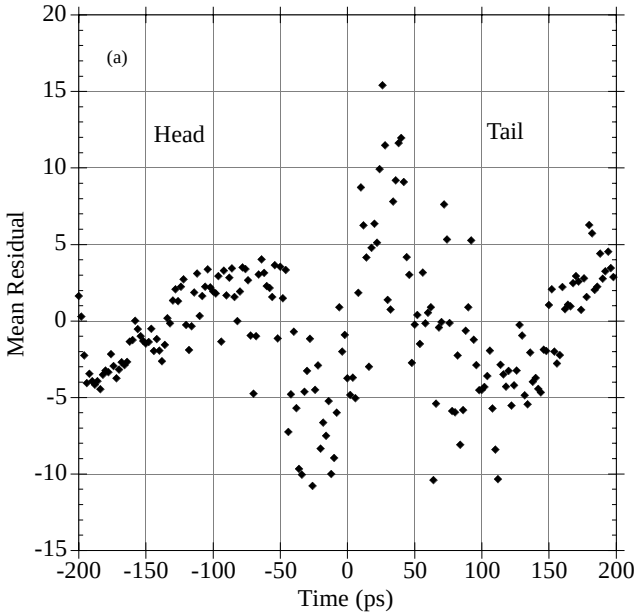

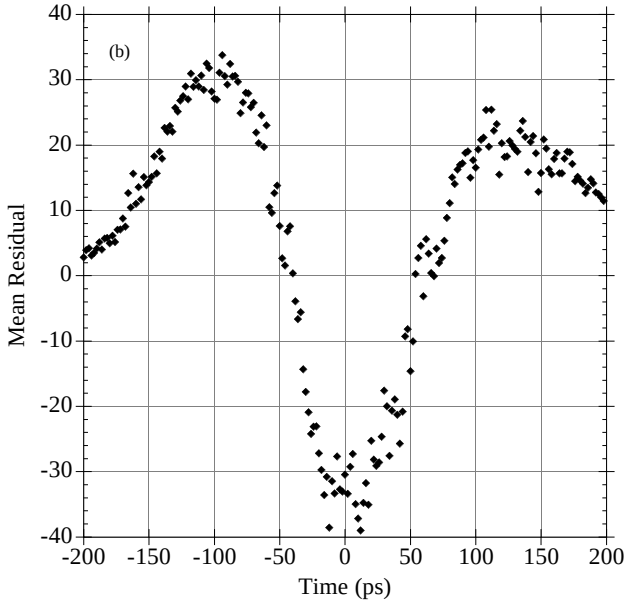

FIG. 14. The mean residual when the phase of the RF voltage was modulated at a voltage amplitude of (a) -20 dBm and (b) +10 dBm and frequency of 369.9 kHz. The head of the bunch is to the left of the center (zero on the plot) and the tail of the bunch is to the right of the center.

4) An effort was made to correlate the signal generator sinewave phase with the streak camera. By locking the streak camera trigger with the signal generator, the phase of the signal generator could be changed, and the phase of the instability would follow the change in the phase. This would enable the streak camera to measure the phase of the induced bunch distribution changes. Figure 15 displays the bunch length as a function of streak camera picture when the streak camera trigger was supposedly phase locked with the signal generator pulse. This effort was unsuccessful, and is evident from the bunch length, due to the lack of correlation between the steak camera and the signal generator.

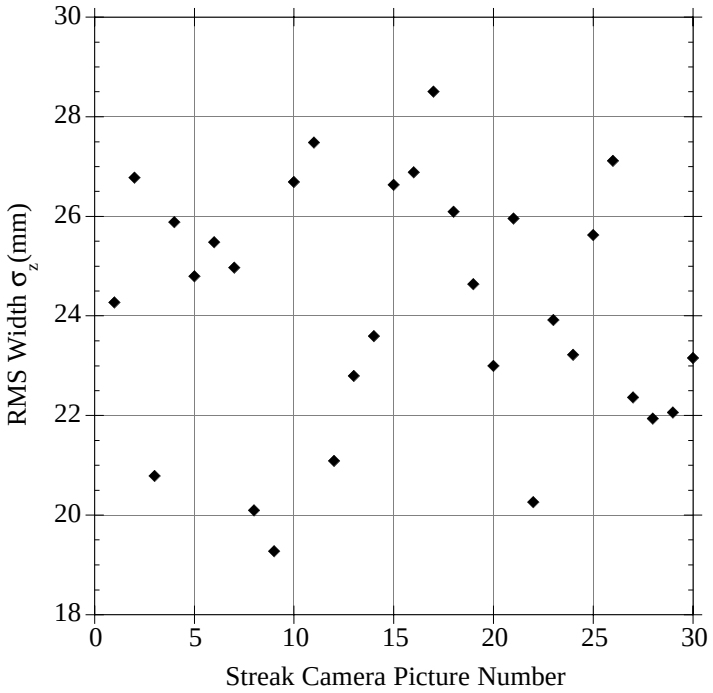

FIG. 15. The bunch length as a function of picture number taken by the streak camera when modulating the RF voltage at a voltage amplitude of +10 dBm and frequency of 369.9 kHz.

b) Quadrupole Mode (m=2)

The quadrupole mode of oscillation was induced in CESR in a single bunch of electrons at a current of approximately 8 mA. The bunch distribution was excited by driving the RF amplitude with a signal generator at 349.9 kHz for three different voltage amplitudes. Figure 16 are typical single data acquisitions of longitudinal bunch distributions when the signal generator voltage was (a) 0 dBm, (c) +5 dBm, and (e) +10 dBm. The distributions were fit to the mean stable distributions and the residual from the fit is plotted in fig. 16.

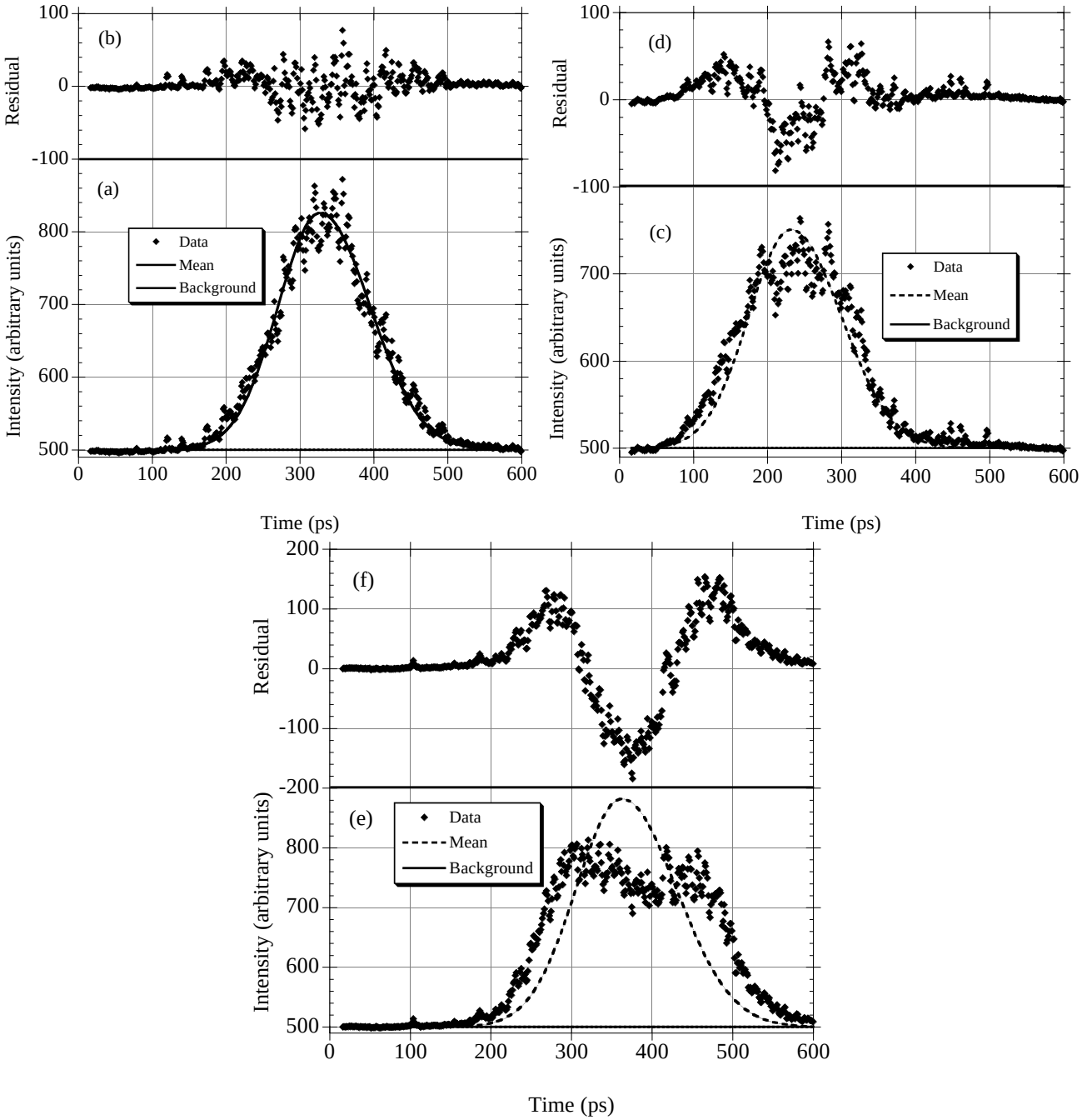

FIG. 16. A single data acquisition of the longitudinal bunch distribution when the amplitude of the RF voltage is modulated at a frequency of 349.9 kHz and signal generator voltage amplitude of (a) 0 dBm, (c) +5 dBm, and (e) +10 dBm. The residual from the mean stable distribution for the above signal voltages of (b) 0 dBm, (d) +5 dBm, and (f) +10 dBm.

Several comments can be made about the results:

1) When driving the quadrupole mode, the dipole mode is always present (table V). The dipole mode amplitude is not as large as the quadrupole mode amplitude, but it is always present.

2) From the mean residuals in fig. 17, a noticeable change in the bunch distribution is present at all three voltage settings. The quadrupole mode appears in the mean residual at all three voltage settings.

The single data acquisitions of the bunch distribution (fig. 16 (c) and (e)) exhibit a dramatic change in the bunch distribution for the +5 dBm and +10 dBm voltage settings.

	0 dBm Sinewave	+5 dBm Sinewave	+10 dBm Sinewave
f_r (390 kHz)	-17 dB	-16 dB	-15 dB
$f_r - f_s$ (369.9 kHz, m=1)	-61 dB	-56 dB	-52 dB
$f_r \pm 2 f_s$ (349.9 kHz, m=2)	-54 dB	-47 dB	-46 dB

TABLE V. The beam spectra amplitudes from the spectrum analyzer when modulating the amplitude of the RF voltage at 349.9 kHz.

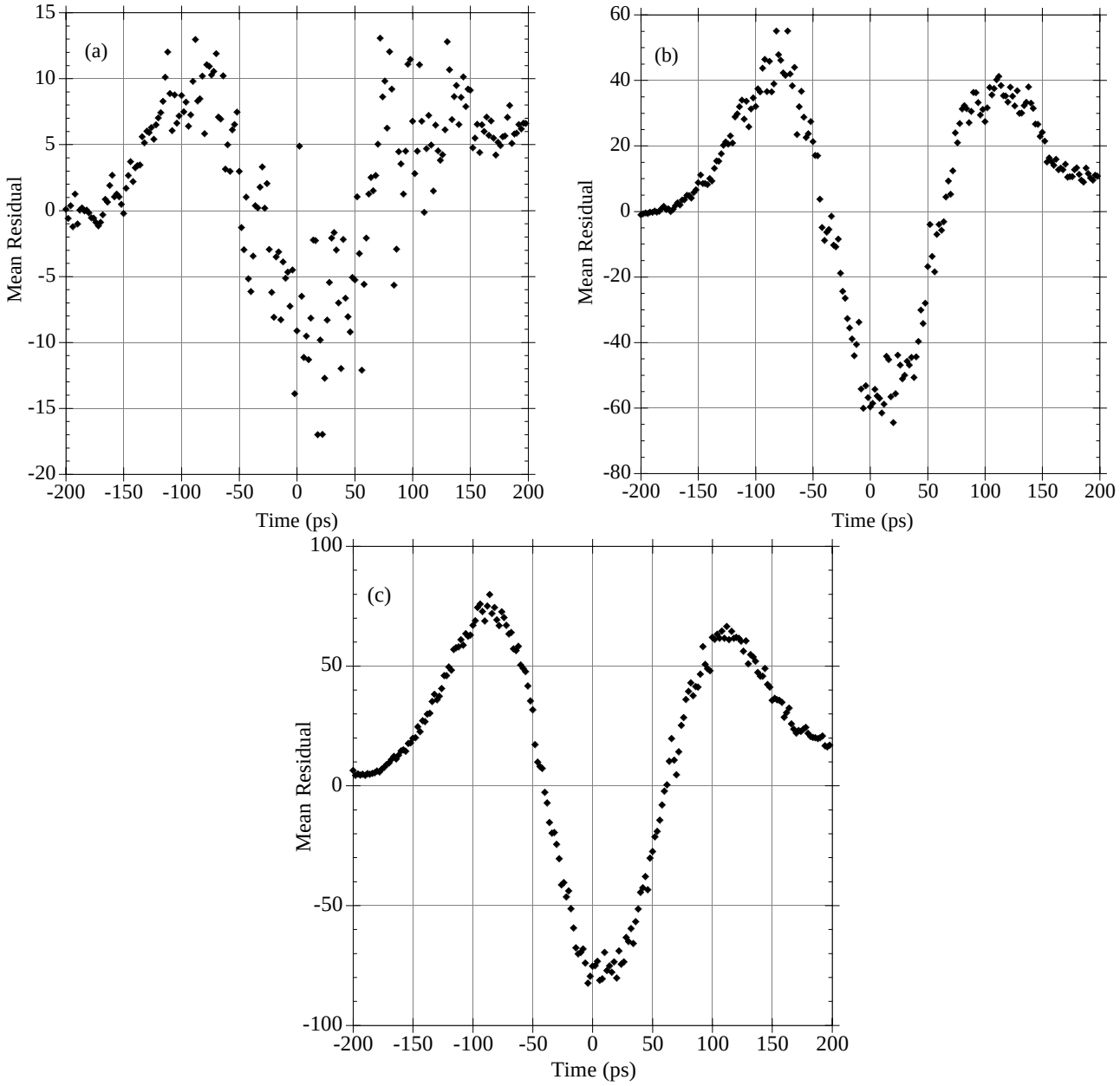

FIG. 17. The mean residual when the amplitude of the RF voltage is modulated at voltage amplitudes of (a) 0 dBm, (b) +5 dBm, and (c) +10 dBm and frequency of 349.9 kHz.

3) The bunch length, bunch width, and asymmetry factor for the three different voltage amplitudes is listed in table VI. Bunch lengthening is observed with an increase in signal generator voltages. The bunch width better describes the bunch length when the quadrupole or higher order mode is present. The bunch width is determined by calculating

$$\text{Width} = \sqrt{\frac{\sum_{i=1}^{N}\left(z_i - \bar{z}\right)^2 I\left(z_i\right)}{\sum_{i=1}^{N} I\left(z_i\right)}}$$

where N is the number of CCD pixels within $\pm 3\sigma$ of the mean $\bar{z}$, z_i is the location of the pixel, and $I\left(z_i\right)$ is the projection height. The bunch length and width in this circumstance is displayed in table VI.

	No Drive	0 dBm Sinewave	+5 dBm Sinewave	+10 dBm Sinewave
RMS Width σ_z	18.46 ± 0.11mm	19.4 ± 0.3mm	23.5 ± 0.6mm	26.6 ± 0.4mm
Mean Width	19.14 ± 0.12mm	20.4 ± 0.3mm	24.8 ± 0.6mm	26.9 ± 0.3mm
Asymmetry Factor	-0.07 ± 0.01	-0.09 ± 0.01	-0.08 ± 0.02	-0.01 ± 0.04

TABLE VI. The bunch length and asymmetry factor when the amplitude of the RF voltage is modulated at a frequency of 349.9 kHz.

c) Sextupole Mode (m=3)

The sextupole mode of oscillation was induced in CESR on a single bunch of electrons at a current of approximately 8 mA. The bunch distribution was driven by modulating the phase of the RF voltage with the signal generator at the frequency of 329.8 kHz and voltage amplitude of +10 dBm. Figure 18 (a) is a typical single data acquisition when the signal generator was set to +10 dBm and the modulated longitudinal bunch distribution was fit to a stable distribution. The residual from the fit is plotted in fig. 18 (b). The bunch length and asymmetry factor for these measurements are $\sigma_z = 18.56 \pm 0.08$ mm and $\text{Asy} = -0.07 \pm 0.01$.

There was no evidence for the quadrupole mode being present when the sextupole mode was driven. The bunch distribution exhibits a small change and the deviation from a stable distribution is less visible in the residual than in the quadrupole case. The head of the longitudinal distribution changes shape slightly and this is observed in a single data acquisition. A bump is visible in the residual (fig. 18 (b)) and in the mean residual (fig. 18 (c)). The deviation from the stable distribution is stronger in the head of the mean residual than in the tail of the residual. Table VII lists the beam spectra amplitudes during the measurement.

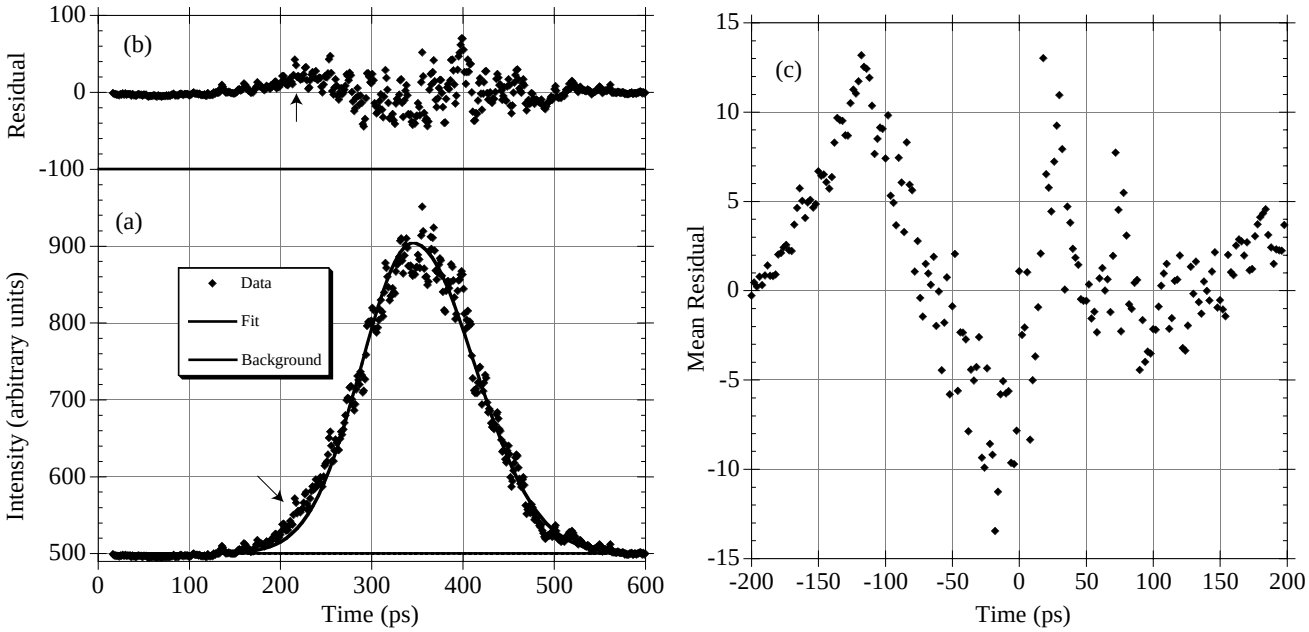

FIG. 18. A single data acquisition of the longitudinal bunch distribution fit to the mean stable distribution when the phase of the RF voltage is modulated at (a) +10 dBm. The residual (b) between the single data acquisition and the mean stable distribution. The mean residual for the data set is plotted in (c). The arrows in (a) and (b) depict the onset of the sextupole mode oscillation in the bunch distribution.

	+10 dBm Sinewave
f (390 kHz, m=0)	-17 dB
$f_r - f_s$ (369.9 kHz, m=1)	-62 dB
$f_r - 2f_s$ (349.9 kHz, m=2)	-
$f - 3f$ (329.8 kHz, m=3)	-52 dB

TABLE VII. The beam spectra amplitudes from the spectrum analyzer when modulating the phase of the RF voltage at 329.9 kHz.

d) Octupole Mode (m=4)

The octupole mode of oscillation was excited in CESR on a single bunch of electrons at a current of approximately 10 mA. The bunch distribution was excited by driving the RF amplitude with a signal generator at a frequency of 309.8 kHz at a voltage amplitude of +10 dBm. Figure 19 is a typical single data acquisition of the modulated longitudinal bunch distribution. The bunch length and asymmetry factor for these measurements are $\sigma_z = 18.35 \pm 0.07\,\text{mm}$ and $\text{Asy} = -0.08 \pm 0.01$. It is interesting to note that with a 10 dBm signal, the same strength that produced major changes in the bunch distribution at 349.9 kHz (quadrupole mode), little evidence of change in the bunch distribution is noticed at 329.9 kHz (sextupole mode) and 309.8 kHz (octupole mode).

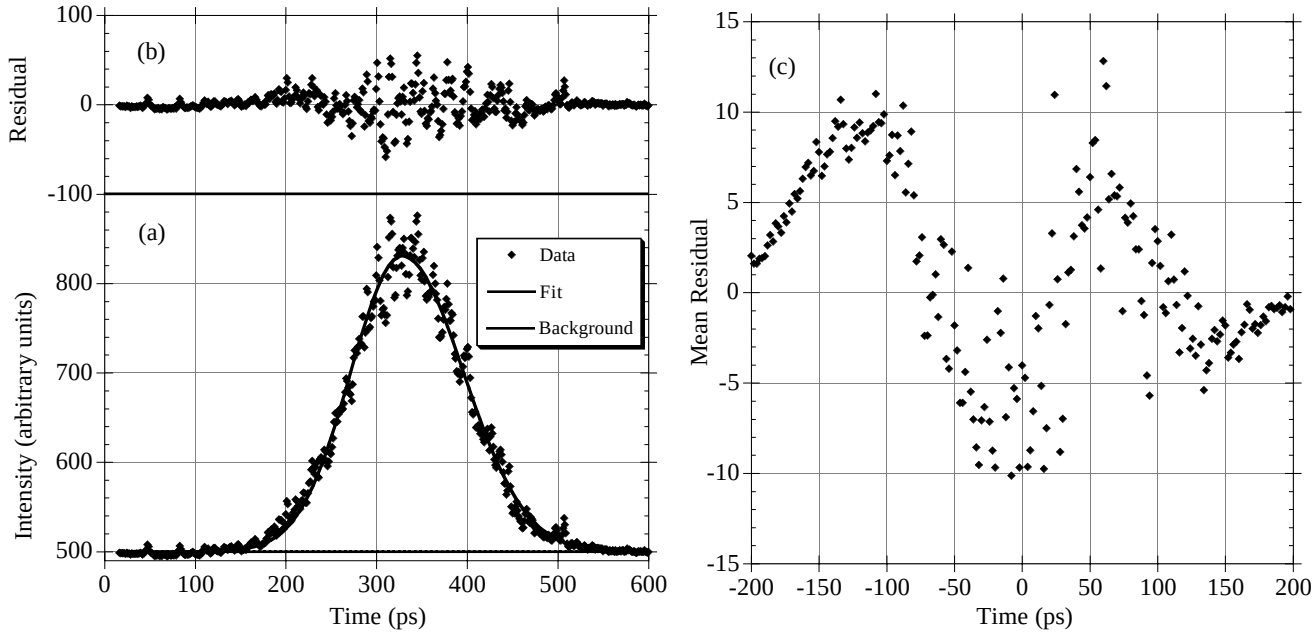

FIG. 19. A single data acquisition of the longitudinal bunch distribution fit to the mean stable distribution when the signal generator voltage is (a) +10 dBm and frequency is 309.9 kHz. The residual from the mean distribution when the signal generator voltage is (b) +10 dBm. The mean residual for the octupole mode is plotted in (c).

From the mean residual, the bunch distribution exhibits a slight deviation from a stable distribution. The quadrupole and sextupole modes were not present when the octupole mode was excited (table VIII).

	+10 dBm Sinewave
f_r (390kHz)	-18 dB
$f_r - f_s$ (369.9 kHz, m=1)	-59 dB
$f_r - 2f_s$ (349.9 kHz, m=2)	-
$f_r - 3f_s$ (329.9 kHz, m=3)	-
$f_r - 4f_s$ (309.9 kHz, m=4)	-52 dB

TABLE VIII. The beam spectra amplitudes from the spectrum analyzer when modulating the amplitude of the RF voltage at 309.9 kHz.

(VI) The Dipole-Coupled-Bunch Mode Instability in CESR

a) Instability Properties

The CESR longitudinal instability is a dipole-coupled bunch instability, which is only observed with multiple bunches per train. The characteristics of the instability are described in detail elsewhere [6]. The threshold of the instability depends upon the mode of operation. We observed that: 1) at the instability threshold current, a signal at $nf_r \pm f_s$ appears in the beams spectra, which indicates a predominately dipole motion in phase space. 2) As the current is increased, well above the instability

threshold, the signal at $nf_r \pm 2f_s$ appears. 3) The threshold current for the instability is dependent on the bunch spacing in the train. 4) The instability degrades the CESR luminosity. Figure 20 (a)-(c) is a plot of the dipole-coupled-bunch instability current thresholds for the various bunch spacings at the time of the streak camera measurements.

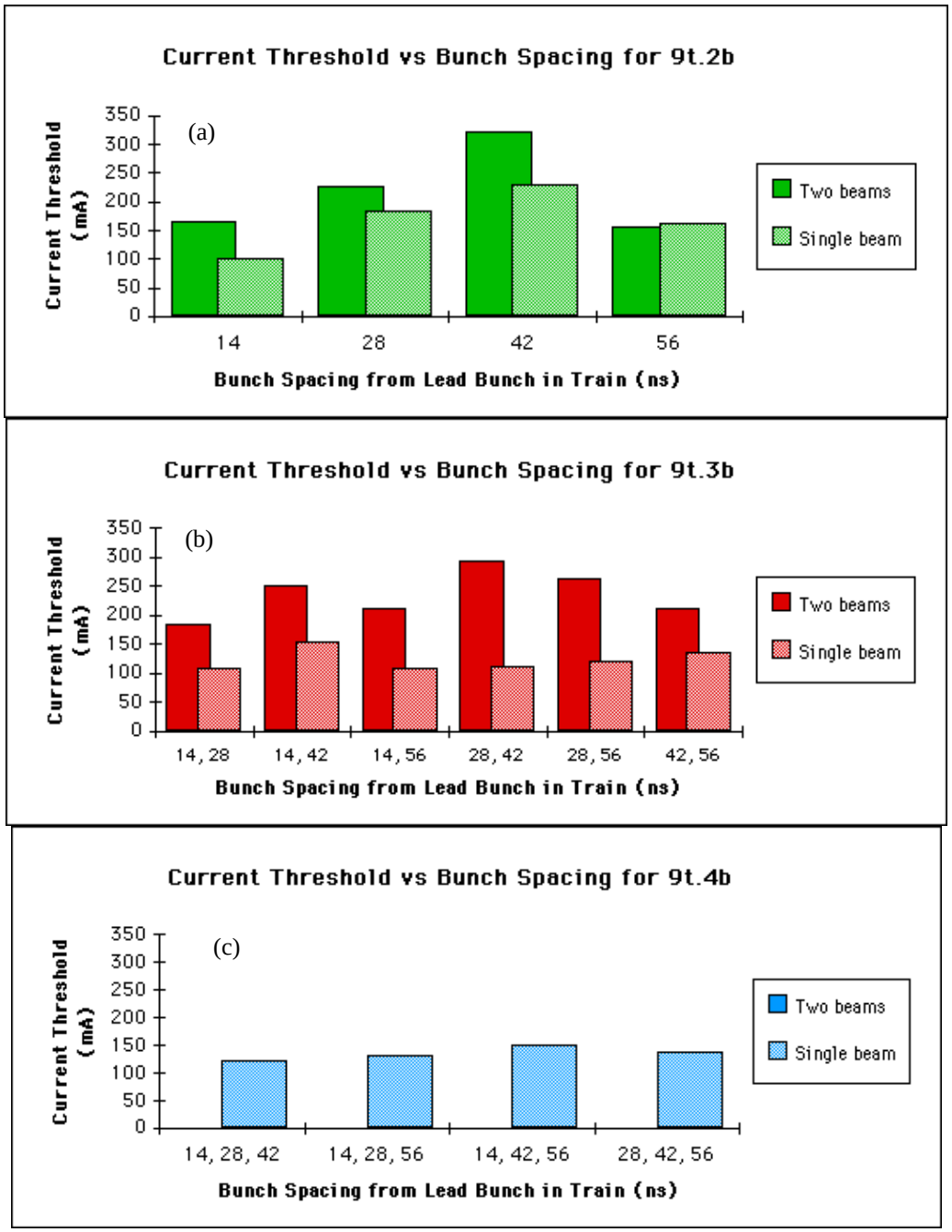

FIG. 20. The current threshold for the dipole-coupled-bunch instability with nine trains of (a) two bunches per train, (b) three bunches per train, and (c) four bunches per train. These measurements were made with the four copper RF accelerator sections in CESR and during the same period when the streak camera measurements were made.

A spectrum analyzer was used in conjunction with the streak camera to measure the amplitude and frequency of the beam spectra. An example of the CESR beam spectrum from a beam position monitor electrode is displayed in fig. 21 (a) and (b). Figure 21 (a) is the beam spectra below the instability threshold when nine trains of two bunches, separated by 56 ns, with a total beam current of 75 mA, is present in CESR. Figure 21 (b) is the beam spectra above the instability threshold when the bunch spacing is 56 ns apart when a total current of 135 mA is present in CESR. The synchrotron sidebands associated with the dipole-coupled-bunch longitudinal instability are clearly visible at $f = nf_r \pm f_s$ (n=5644 in this case).

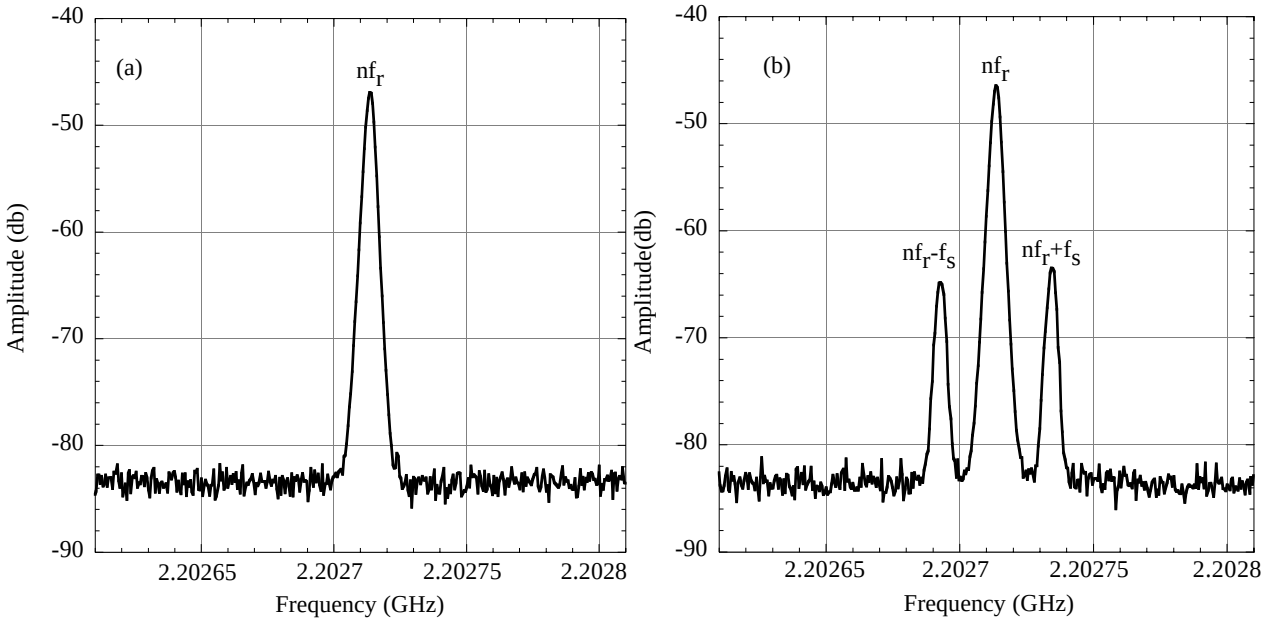

FIG. 21. The spectrum analyzer beam spectra centered on a rotation harmonic at 2.20271 GHz (a) without the instability and (b) with the instability present. The synchrotron frequency for CESR is f_s~20kHz.

Measurements of the bunch distribution at several different bunch spacings were made with the dipole-coupled-bunch longitudinal instability present. The longitudinal feedback system, which at the time of the measurements, consisted of a horizontal kicker magnet that damps the dipole longitudinal oscillations using local dispersion, was not fully operational during these measurements[7]. At the time of the measurements, normal high-energy physics configuration was nine trains and 42 ns spacing. This bunch spacing mode was chosen for its high current threshold (fig. 20 (a)). The current threshold at this bunch spacing was not obtainable during the streak camera measurements due to heating of the vacuum chamber. Other bunch spacing configurations were chosen to observe the dipole-coupled-bunch longitudinal instability.

b) Nine trains with two bunches separated by 14 ns.

The longitudinal coupled bunch instability has a low current threshold in CESR with nine trains of two bunches with 14 ns spacing. With this bunch spacing the single beam instability current

threshold was approximately 110 mA. For these measurements the RF accelerating voltage was 6.31 ± 0.01 MV and the wiggler magnets were closed. Just above the instability threshold, measurements of the electron bunch distribution were taken with the streak camera with the feedback on (no instability present), and with the longitudinal feedback off (instability present). Figures 22 (a) is a typical single data acquisition of the longitudinal bunch distribution taken with the streak camera with the feedback off and the dipole-coupled-bunch instability present. The instability was noted by the appearance of a signal at $f_r - f_s$ (369.9 kHz) in the beam spectra. The distribution was fit to the mean stable distribution and the residual is plotted above the distribution. Figure 22 (b) is a typical single data acquisition of the longitudinal bunch distribution with the feedback on and declared stable in the beam spectra. The stable bunch distribution was also fit to the mean stable bunch distribution to exhibit the pulse-to-pulse fluctuations of the distribution and streak camera.

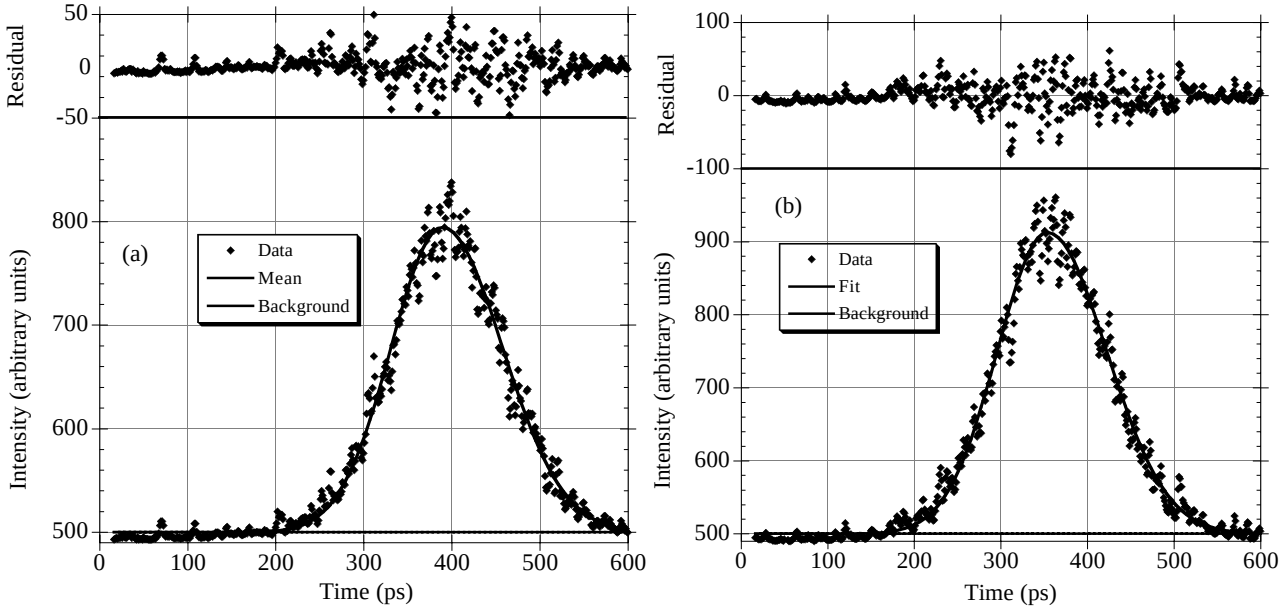

FIG. 22. A single data acquisition of the electron longitudinal bunch distribution measured by the streak camera when (a) the longitudinal feedback is off and the longitudinal instability present and (b) the longitudinal feedback is on and the longitudinal instability not present. The residual when the instability was present (c), and not present (d).

The mean bunch length and asymmetry factor from the fit to the data is listed in table IX.

	Feedback On	Feedback Off
RMS Width σ_z	18.78 ± 0.13mm	18.73 ± 0.09mm
Asymmetry Factor	-0.07 ± 0.01	-0.07 ± 0.01

TABLE IX. The electron bunch length and asymmetry factor when the instability is present (feedback off) and not present (feedback on).

The features of the longitudinal instability from the measurement are the following:

1) As in the case when the dipole oscillator is excited by the RF system the dipole mode is not detectable by the streak camera when the instability was present just above the instability threshold. The bunch length and asymmetry factor is in good agreement with each other with and without the instability present.

2) No structure is detected in the single data acquisition residuals or the mean residuals. Figure 23 is the mean residual with and without the instability present. There appears to be more structure in the residual when the instability was not present.

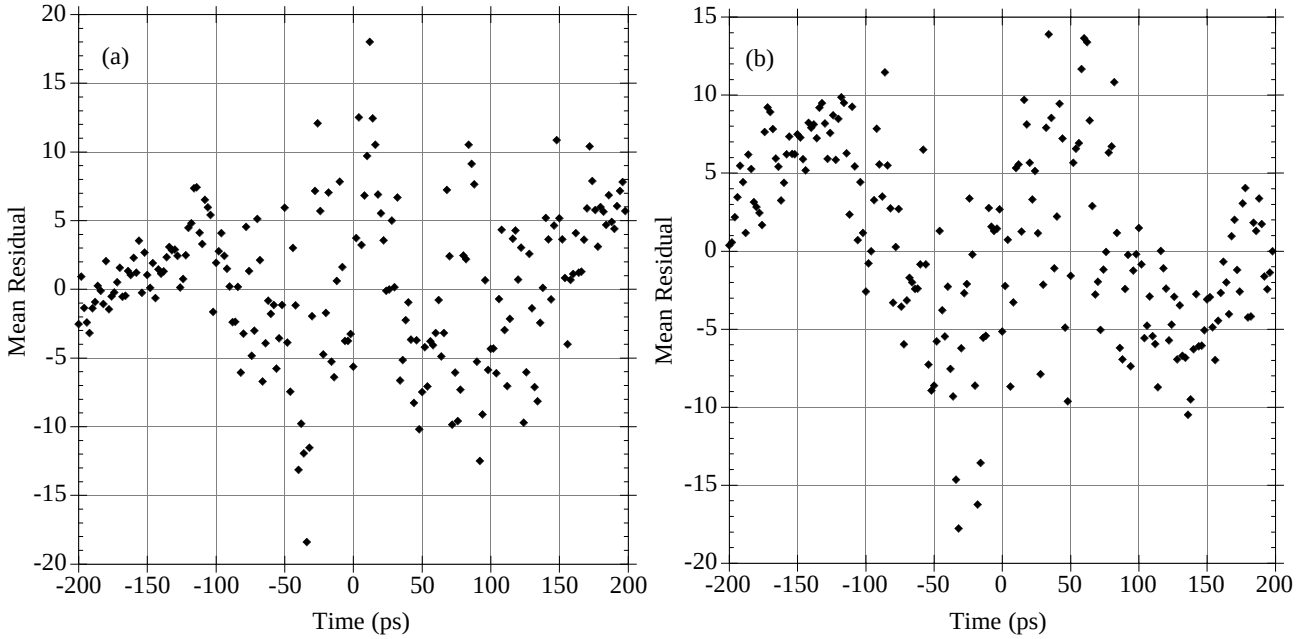

FIG. 23. The mean residual with the instability (a) present and (b) not present.

Exploring the instability behavior further, the current was increased to approximately 210 mA. Increasing the current caused several interesting features to appear:

1) The longitudinal feedback system was not able to damp the beam above 130 mA of total current. The $f_r \pm f_s$ signal appeared in the beam spectra regardless of the longitudinal feedback.

2) Figure 24 (c) is the bunch length as a function total current between 170 and 210 mA. The bunch length increases dramatically with current, and it oscillates in size. This is a signature of the quadrupole-coupled-bunch instability or a dipole oscillator driven to large amplitude.

3) As the current increases, the $f_r \pm 2 f_s$ signal appears in the beam spectra. The $f_r \pm 2 f_s$ signal growth in strength is evident in fig. 24 (c). There is a dramatic jump in the $f_r \pm 2 f_s$ signal amplitude when the longitudinal distribution changes dramatically.

4) With this increase in current, similar behavior in the longitudinal bunch distribution is observed as with increasing the RF modulation voltage amplitude in previous experiments. As the current increases, the wake voltage in the RF cavities becomes stronger, and excites the quadrupole mode, and changes the bunch distribution dramatically. The bunch distribution oscillates violently above 195 mA and that is evident in fig. 24 (a) and (b). The bunch distributions are fit to the stable bunch

distribution and the residual is then computed and plotted above the distribution. Figure 24 (a) and (b) are two typical single data acquisitions of the longitudinal bunch distributions at a total current of 200 mA. In figure 24 (a), there is strong evidence of the quadrupole mode, and in fig. 24 (b), there is little evidence of the quadrupole mode.

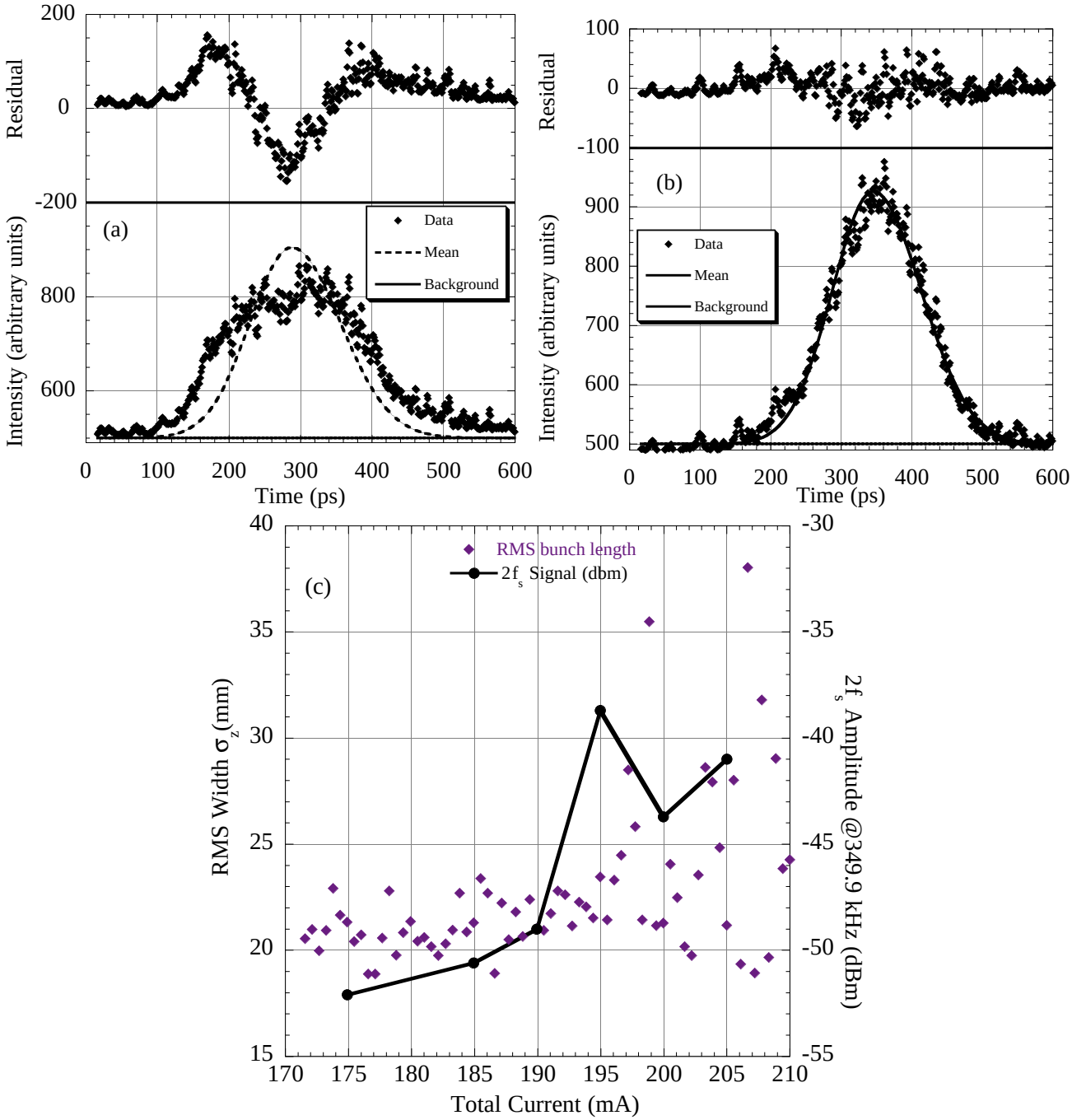

FIG. 24. (a)-(b) A single data acquisition of the longitudinal bunch distribution fit to the mean stable bunch distribution when the beam is unstable. The beam spectra signals of $f_r \pm f_s$ and $f_r \pm 2f_s$ are present and beam current is 200 mA during the measurement. These are two consecutive pictures of the bunch distribution and the current difference between the pictures is not more than one mA. The

residuals are plotted above the distribution. (c) The bunch length and $2f_s$ spectra amplitude as a function of current.

5) The strength of the instability is evident in the mean residual. The mean residual is plotted in fig. 25 for three different currents in CESR. The amplitude of the mean residual exhibits the strength of the quadrupole-coupled-bunch instability and it lessens as the current decreases.

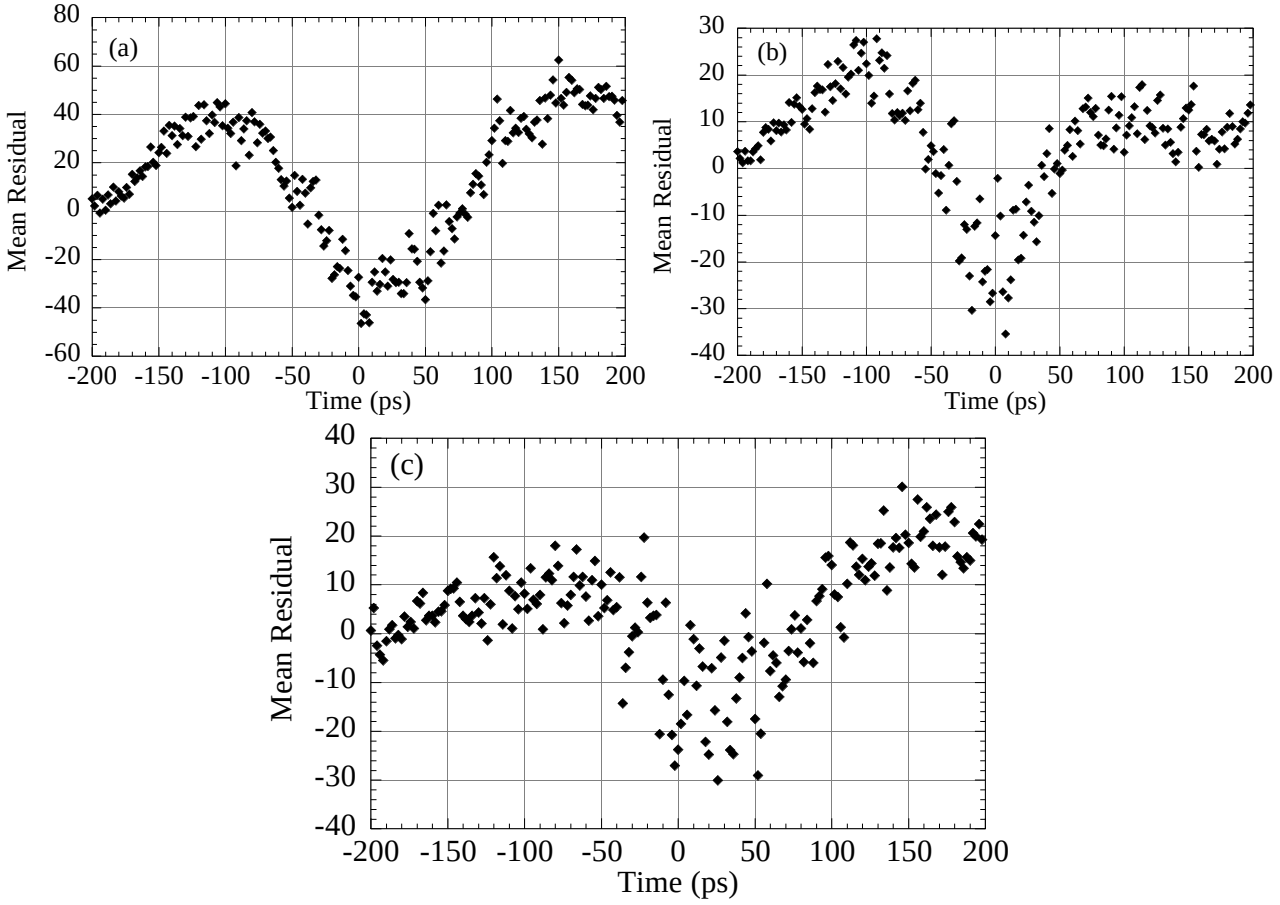

FIG. 25. The mean residual when the total current was between (a) 210-205 mA, (b) 195-188 mA, and (c) 175-171 mA.

c) Nine trains with 3 bunches per train with bunch spacing of 28 ns and 14 ns.

Higher luminosity is achieved by colliding higher total beam currents. Higher beam currents can be achieved in several ways. The method chosen for CESR is to add more bunches in a train. This spreads the total current out over many bunches and reduces the intrabunch transverse and longitudinal wakefields by reducing the total single bunch current. One of the goals now at CESR is to increase the number of bunches per train by having many bunches with low current rather than fewer bunches with high current.

With this in mind the dipole-coupled-bunch longitudinal instability was measured with the streak camera with nine trains of bunches, that consist of three bunches in the train. The bunch spacing between bunch #1 and #2 was 28 and between bunch #2 and #3 was 14 ns. With this bunch spacing

the dipole-coupled-bunch longitudinal instability threshold is approximately 125 mA. For these measurements the RF accelerating voltage during these measurements was 6.51 ± 0.01MV, and the wiggler magnets were closed. Just above the instability threshold the electron bunch distribution was measured with the streak camera with the feedback on and no instability present, and with the feedback off with the instability present. Figure 26 (a) is a typical single data acquisition of the longitudinal bunch distribution taken with the feedback off and the dipole-coupled-bunch instability present. Once again, the instability's presence was determined by the presence of the $f_r \pm f_s$ signal in the beam spectra. Figure 26 (b) is a typical single data acquisition of the longitudinal bunch distribution with the feedback on and the instability is not detected in the beam spectra with the longitudinal feedback on.

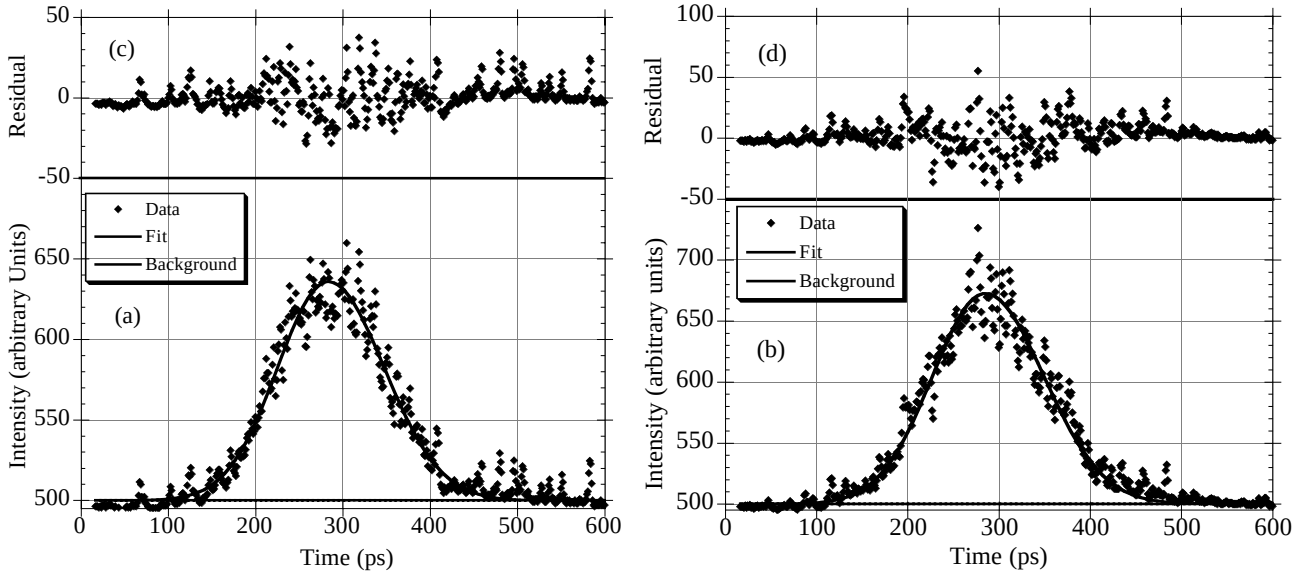

FIG. 26. A single data acquisition of the electron longitudinal bunch distribution measured by the streak camera when (a) the longitudinal feedback is off and the longitudinal instability is present and (b) the longitudinal feedback is on and the longitudinal instability is not present. The residual from the fit is plotted when the instability was present (c) and not present (d)

The measured bunch length and asymmetry factor from the fit to the data is listed in table X.

	Feedback On	Feedback Off
RMS Width σ_z	18.04 ± 0.24mm	18.20 ± 0.27mm
Asymmetry Factor	-0.07 ± 0.01	-0.07 ± 0.03

TABLE X. The electron bunch length and asymmetry factor when the instability is present (feedback off) and not present (feedback on).

Much like the two bunches per train case, with three bunches per train: 1) The dipole mode is not detectable by the streak camera. The bunch length and asymmetry factor is in good agreement with each other with and without the dipole-coupled-bunch instability present. 2) No structure was

detected in the residuals or the mean residuals. Figure 27 is the mean residual with and without the instability present.

The background in the streak camera images have a larger noise component with the three bunches present per train. This increase in noise is due to an extra bunch per train. A reduction in noise for future experiments can be achieved by using a light chopper.

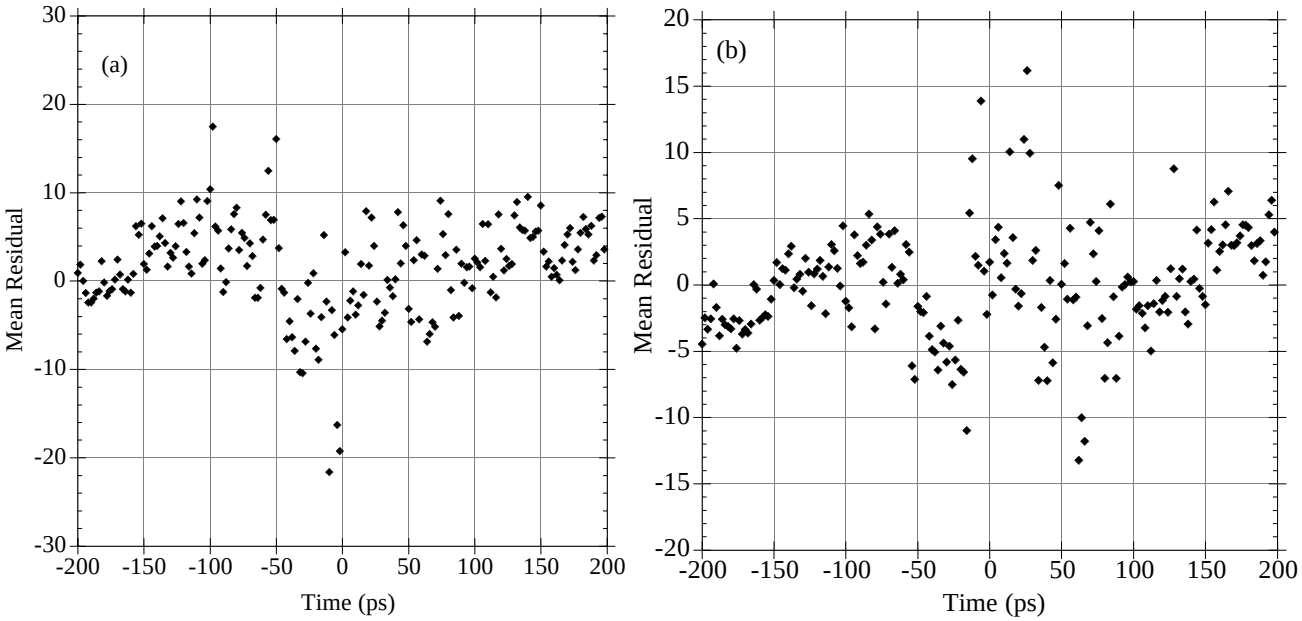

FIG. 27. The mean residual with the instability (a) present and (b) not present.

The current was increased and several interesting features appeared:

1) Identical to the two bunches per train case, the longitudinal feedback system was not able to damp the beam above 130 mA of total current. The instability was too strong, the $f_r \pm f_s$ signal would appear in the beam spectra independent of the feedback system.

2) There is a steady increase in the bunch length as a function of current. As the current increases, the $f_r \pm f_s$ and $f_r \pm 2 f_s$ signals appear and grow in strength in the beam spectra as a function of current. In fig. 28 (c) the dipole ($f_r \pm f_s$) and quadrupole ($f_r \pm 2 f_s$) signal amplitudes are plotted, as well as the bunch length.

3) As the current is increased even higher (fig. 28 (d)), the bunch distribution oscillates with a similar violate behavior as seen in the two bunch per train case. Figure 28 (a) is a typical single data acquisition of the bunch distribution at 170 mA of total current in CESR. The bunch distribution is fit to the stable bunch distribution and the residual is plotted above the distribution. The residual in fig. 28 (a) does not exhibit the quadrupole mode. At higher current the quadrupole mode is evident, as in Fig. 28 (b), and it looks similar in structure to the theoretical distribution in fig. 4 (b).

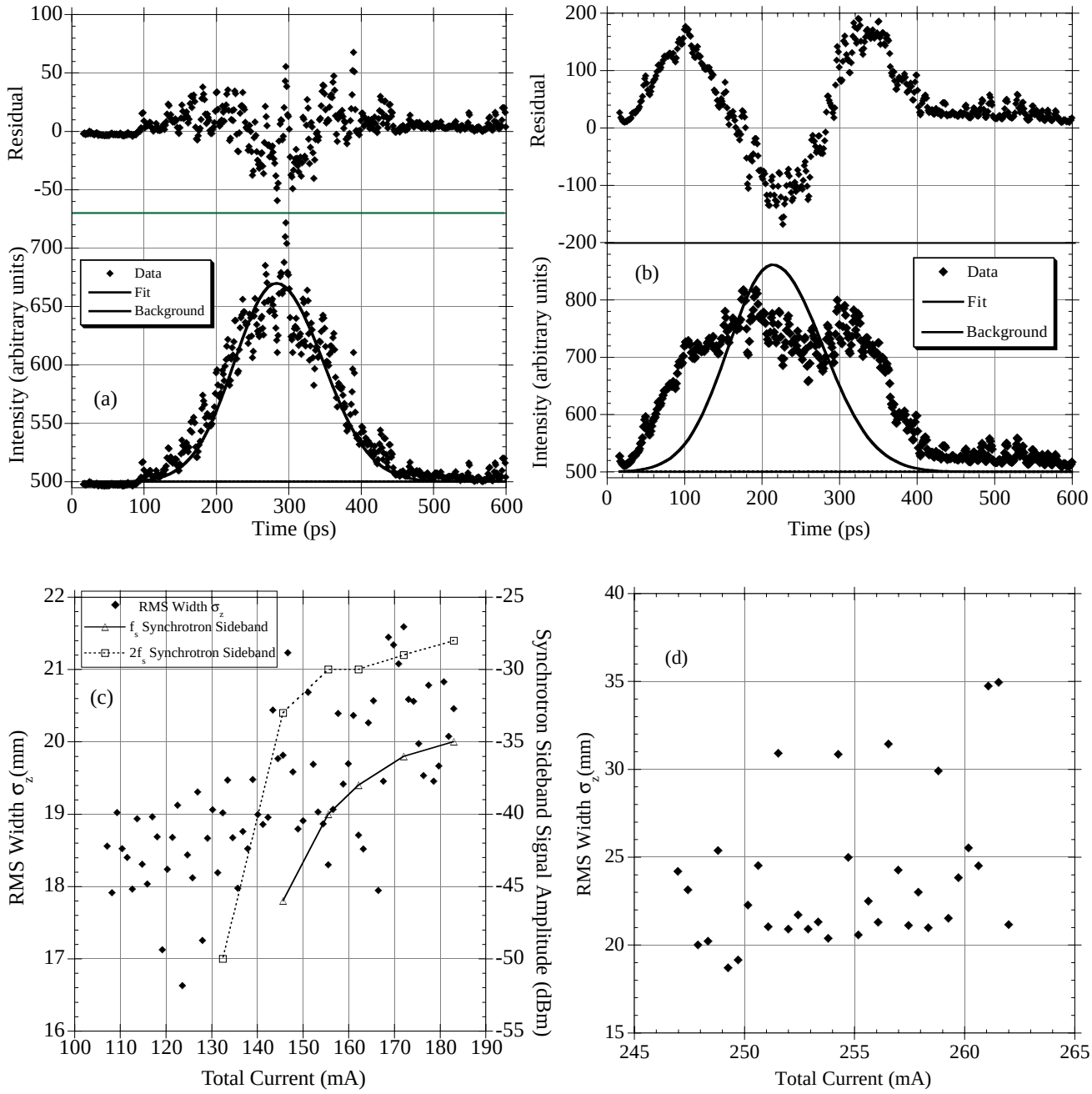

FIG. 28. (a) A single data acquisition of the longitudinal bunch distribution fit to the mean stable bunch distribution. The beam is declared unstable due to the presence of the $f_r \pm f_s$ and $f_r \pm 2f_s$ signals in the beam spectra. The current is 170 mA total. The residual between the distribution and the fit is plotted above the distribution. (c) The bunch length and synchrotron sideband amplitudes for $f_r \pm f_s$ and $f_r \pm 2f_s$ signals between the current of 183-105 mA. (d) The bunch length between the current of 262-247 mA. The amplitude of the beam spectra was not measured during this experiment but the $f_r \pm f_s$ and $f_r \pm 2f_s$ signals were present during the measurement.

4) The mean residual is plotted in fig. 29 (a) and (b) for the two different current ranges. In both cases the quadrupole-coupled-bunch instability is evident.

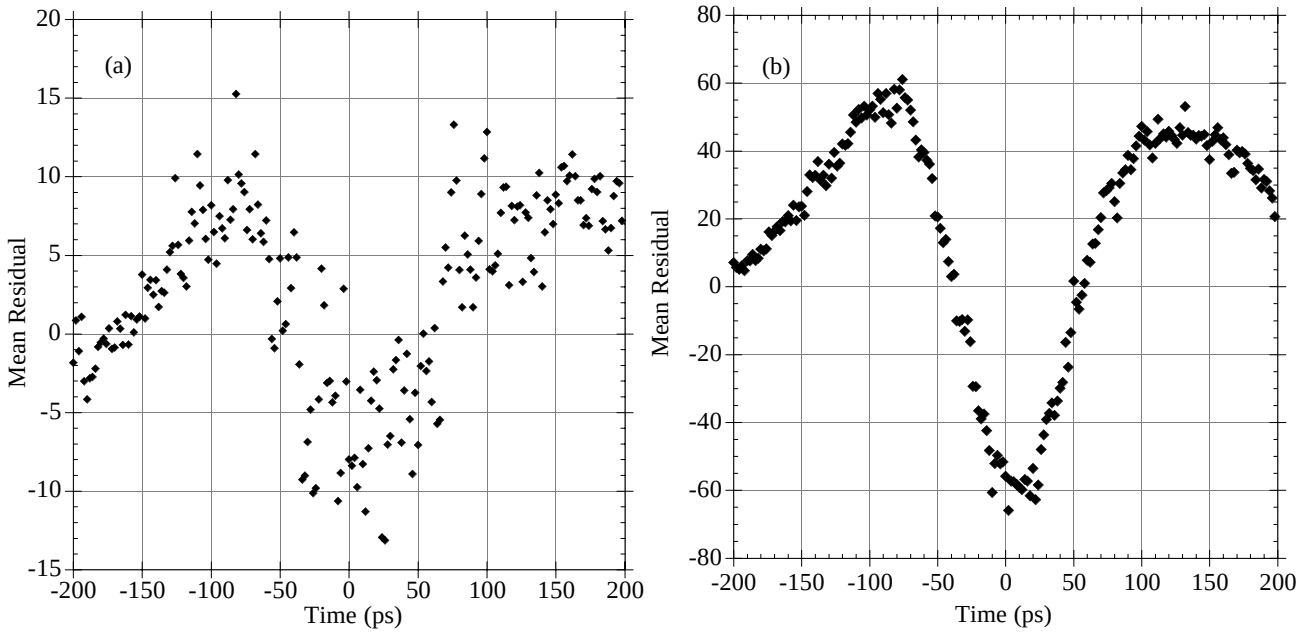

FIG. 29. The mean residual of the bunch distributions between the current of (a) 183-160 mA, and (b) 262-247 mA.

5) From these measurements it appears that there is no real advantage to nine trains with three bunches over nine trains with two bunches. With the normal conducting copper RF cavities, the highest measured current threshold is with two bunches separated by 42 ns. The dipole-coupled-bunch longitudinal instability exhibits the same behavior for all bunch configurations.

5. Conclusions

The measurements of CESR provide information about the behavior of the bunch during multiple bunch operations, when the dipole-coupled-bunch longitudinal instability was present in CESR. The general conclusions from the measurements are that in terms of longitudinal dynamics there is no difference between the positrons and electrons in CESR. The coupled-bunch longitudinal instability is a dipole mode instability, which may be damped by a strong feedback system thereby increasing the current threshold [7]. The presence of the longitudinal instability is detected in the beam spectra. It was also detected with the streak camera but only when the quadrupole mode was present.

These studies of the longitudinal dynamics in CESR helped quantify some effects, such as: 1) the bunch length and asymmetry of the bunch increases as a function of current while colliding beams. 2) The bunch length increases as a function of current with multiple bunches in CESR. 3) Modulation of the RF voltage on a single bunch can be used to simulate the behavior of the coupled-bunch instability. The change in the bunch distribution detected by the beam spectra is correlated with the distribution changes measured by the streak camera. 4) There is essentially no change in the bunch distribution due to the pretzel orbit or wiggler magnets. 5) With 42 ns spacing between bunches the first bunch in the train is slightly longer than the second bunch in the train. This could be important

when bunches are separated by 14 ns in future colliding beam configurations. 6) The theoretical bunch length with the wiggler magnets open and closed closely match the measured results. 7) The coupled bunch longitudinal instability is a dipole instability, but when the current is increased, it excites the quadrupole oscillation at which time the bunch distribution changes drastically. Nonlinearites in the potential well and the large amplitude motion in the dipole mode give rise to the quadrupole mode. With the present feedback system the coupled bunch instability is eliminated at currents above threshold for the quadrupole oscillation being present.

The streak camera has been invaluable as a diagnostic device for the measurement of the longitudinal parameters for CESR. There is no other tool at CESR has the capability to measure the bunch distribution to the same accuracy.

6. Acknowledgments

The authors would like to thank the Stanford Linear Accelerator Center for the loan of the streak camera, especially Robert Siemann and Boris Podobedov. We would also like to thank the CESR technicians for there help getting the experimental area ready for the camera, the machine shop for making the copper mirror, the vacuum group for designing and installing the mirror, and Gerry Codner for helping with the RF modulation measurements.

7. References

[1] Holtzapple, R.L., et al.,"Single Bunch Longitudinal Measurements at the Cornell Electron-Positron Storage Ring," Published in: Phys. Rev. ST Accel. Beams 3, 034401, 2000.

[2] Chao, A.W.,*"Physics of Collective Beam Instabilities in High-Energy Accelerators*", New York, USA:Wiley (1993) 371p.

[3] J.L. Laclare, 11th International Conference of High-Energy Accelerators, Basel:Birkhauser Verlag(1980), edited by W.S. Newman, 526p.

[4] Siemann, R.H.,"Bunched Beam Diagnostics", CLNS 89/878, January 1989. 42pp.

[5] James,F., M. Roos,"'Minuit' A System for Function Minimization and Analysis of the Parameter Errors and Correlations", CERN-DD/75/20, Jul 1975. 38 pp. Computer Physic Commun. **10** (1975) 343-367.

[6] Billing, M., "Observation of a Longitudinal Coupled Bunch Instability with Trains of Bunches in CESR," CLNS 98/1564.

[7] Sikora, J., et al, "Longitudinal Feedback at CESR", Presented at the 18th Particle Accelerator Conference (PAC99), New York City, New York, 29 March-2 April 1999.